



**ELUCIDATION OF STRUCTURE – PROPERTY CORRELATIONS USING  
EXPERIMENTAL NUCLEAR MAGNETIC RESONANCE (NMR) AND FOURIER  
TRANSFORM INFRARED (FTIR) SPECTROSCOPY ANALYSIS, AND DENSITY  
FUNCTIONAL THEORY (DFT) CALCULATIONS OF THE DIFURYLMETHANE  
(DFM) MOLECULE, AND DIFURYLMETHANE-METHANOL CLUSTERS**

---

By

**Kago Dikomang**

Kago.Dikomangk@mopipi.ub.bw (+267) 75366278

BSc General (Chemistry & Mathematics) University of Botswana, 2013

**Department of Chemistry**

**University of Botswana**

A dissertation Submitted to the Faculty of Science in Partial Fulfillment of the  
Requirements for the Award of the Degree of Master of Science in Physical Chemistry

**Principal Supervisor:** Baagi Thema-Mmereki, PhD

**Co-Supervisor:** Wilfred Ddamba, PhD

February 2019

## **COPYRIGHT AND DECLARATION**

“I hereby declare that the dissertation submitted for a Master of Science Degree in Chemistry at the University of Botswana, is my own original work and has not been previously submitted to any other institution and any work quoted is indicated and acknowledged by means of a comprehensive list of references.”

---

KAGO DIKOMANG (ID number: 200102106)

Date...../...../2019

© 2018 UB. All rights reserved

## **CERTIFICATION**

The undersigned certify that they have read and hereby recommends for acceptance by the Faculty of Science a dissertation/thesis titled *“ELUCIDATION OF STRUCTURE – PROPERTY CORRELATIONS USING EXPERIMENTAL NUCLEAR MAGNETIC RESONANCE (NMR) AND FOURIER TRANSFORM INFRARED (FTIR) SPECTROSCOPY ANALYSIS, AND DENSITY FUNCTIONAL THEORY (DFT) CALCULATIONS OF THE DIFURYLMETHANE (DFM) MOLECULE, AND DIFURYLMETHANE-METHANOL CLUSTERS”*, in fulfillment of the requirements for the degree of Master of Science in Physical Chemistry at University of Botswana.

**Dr. Baagi T. Mmereki. PhD**

.....

**(Principal Supervisor)**

**Dr. Wilfred Ddamba. PhD**

.....

**(Co-Supervisor)**

Date...../...../2019

## **ACKNOWLEDGEMENTS**

My sincere thanks go to my MSc supervisor Dr. Baagi T. Mmereki for his inspirational instructions, patient guidance and endless source of knowledge to my thesis.

I would also like to acknowledge members of my research committee Dr. Wilfred Ddamba as a Co-Supervisor and Dr. Thabo T. Mokoena as a member for their guidance and comments.

Especially I acknowledge Dr. Zibo G. Keolopile who is a Chemical Physicists for instructions, discussions and comments on matters relating to computational chemistry.

I also feel indebted to my financial support by the University of Botswana Foundation and the Department of Chemistry for making this journey possible.

Last, my great gratitude goes to my family for their support and patience during my research period.

## **DEDICATION**

To my late grandmother Mrs. Keleofile Dikomang.

# CONTENTS

COPYRIGHT AND DECLARATION.....	i
CERTIFICATION .....	ii
ACKNOWLEDGEMENTS.....	iii
DEDICATION.....	iv
CONTENTS.....	v
LIST OF TABLES.....	vii
LIST OF FIGURES .....	ix
ABSTRACT.....	x
1 INTRODUCTION.....	1
1.1 Scope of the Study.....	2
1.2 Objectives.....	3
1.3 Intermolecular Interactions .....	3
1.3.1 Molecular Structural Parameters.....	5
1.3.2 Binding Energies.....	6
1.3.3 Molecular Vibrations / Infrared Spectral Analysis .....	7
1.3.4 Natural Bond Orbital (NBO) Analysis .....	8
1.3.5 Molecular electrostatic potential (MEP) map.....	9
1.3.6 AIM Analysis.....	9
1.3.7 Molecular Mechanics (MM) and Ab-initio study of DFM-n-propanol .....	10
2 METHODOLOGIES.....	10
2.1 EXPERIMENTAL METHODS.....	10
2.1.1 Materials and purification of solvents.....	10
2.1.2 Purification of solvents .....	10
2.1.3 Preparation of the difurylmethane (DFM) .....	11
2.1.4 Sample preparation for NMR Analysis.....	13
2.1.5 Sample preparation for IR spectral analysis .....	13
2.2 COMPUTATIONAL METHODS.....	13
2.2.1 Hartree-Fock (HF) .....	13

2.2.2	Density Functional Theory (DFT) .....	15
2.2.3	The Formulation of Basis Sets .....	16
2.2.4	Equilibrium structures.....	18
2.2.5	Polarizability and dipole moment .....	20
3	RESULTS AND DISCUSSION.....	24
3.1	Equilibrium structures .....	24
3.2	Infrared spectral data.....	28
3.3	Gauge Independent Atomic Orbital (GIAO) calculated chemical shifts and 1-dimensional experimental proton nuclear magnetic resonance (1-Dimensional <sup>1</sup> H-NMR) chemical shifts.	34
3.4	Geometric Parameters of DFM-Methanol adducts .....	41
3.4.1	Molecular electrostatic potential map.....	45
3.4.2	Potential Energy Surface (PES) Scan .....	46
3.4.3	Natural Bond Orbital Analysis.....	51
4	SUMMARY & CONCLUSIONS .....	53
	References.....	54
	Appendices:.....	62
	Appendix A. Conformers of DFM.....	62
	Appendix B. Conformers of DFM-Methanol obtained from relaxed potential energy scan .....	63

## LIST OF TABLES

<b>Table 1.1:</b> Classification of Hydrogen Bonds [19] .....	4
<b>Table 2.1:</b> Experimental (measured using microwave spectroscopy) and theoretical equilibrium structure for Furan bond lengths in angstroms optimized at different levels of theory and basis sets (in Å). Calculations in this work were performed using B3LYP/6-31+ (3d, 3p) .....	19
<b>Table 2.2:</b> Experimental (measured using microwave spectroscopy) and theoretical equilibrium structure for Furan bond angles optimized at different levels of theory and basis sets in degrees (θ). Calculations in this work were performed using B3LYP/6-31+(3d,3p). .....	21
<b>Table 2.3:</b> Equilibrium geometry and dipole moment for furan calculated at different levels of theory with 6-31G** basis set.....	22
<b>Table 2.4:</b> Polarizability components for furan calculated as different levels of theory and basis sets.....	23
<b>Table 2.5:</b> Experimental and Theoretical dipole moment (μ) of furan calculated using different model chemistries .....	23
<b>Table 3.1:</b> Equilibrium bond distance (re) of DFM calculated at B3LYP/6-31+G (3d, 3p) in Angstroms .....	25
<b>Table 3.2:</b> Equilibrium bond angles (θe) of DFM calculated at B3LYP/631+G(3d,3p) in degrees .....	26
<b>Table 3.3:</b> Different energetics of 4 conformers of DFM molecule.....	27
<b>Table 3.4:</b> Experiment and calculated Harmonic frequencies and intensities calculated at B3LYP +G 631(3d, 3p), DFM molecule .....	32
<b>Table 3.5:</b> NMR chemical shifts obtained from experimental and calculated at B3LYP/IGLO-2 for DFM MOLECULE. TMS, $\sigma_{\text{iso}}=32.0092$ (IUPAC numbering system is represented as H-3, H-4, H-5 and H-6 and are highlighted) .....	39
<b>Table 3.6:</b> Theoretical NMR nuclear coupling constants.....	39
<b>Table 3.7:</b> 1H-NMR (300 MHZ NMR data for difurylmethane in CDCl3) .....	39
<b>Table 3.8:</b> The calculated O-H bond in the DFM-MeOH complex and intermolecular bond distance and bond angles. ....	44
<b>Table 3.9:</b> Calculated binding energy (BE <sup>a</sup> ), Counterpoise energy ( $\Delta E^{\text{CP}}$ ) <sup>b</sup> , Energy for Methanol (E <sup>c</sup> ) and DFM (E <sup>d</sup> ) monomers in DFM-MeOH complex geometry and Enthalpy of formation ( $\Delta H$ ) <sup>f</sup> and Gibbs free energy in kcal/mol .....	44



<b>Table 3.10:</b> Potential energy data points $\sigma$ -type (structure A) furan-methanol complex obtained by performing rigid (manual) scan .....	48
<b>Table 3.11:</b> Potential energy data points $\pi$ -type (structure B) furan-methanol complex obtained by performing redundant scan .....	49
<b>Table 3.12:</b> The stabilization energy, Fock-matrix and energy gap between HOMO and LUMO orbitals.....	52
<b>Table 3.13:</b> The atomic charges of DFM-MeOH complex .....	52

## LIST OF FIGURES

<b>Figure 1.1:</b> Structure of difuryl methane.....	2
<b>Figure 1. 2: Schematic of Hydrogen bonding showing donor acceptor rearrangement .....</b>	<b>4</b>
<b>Figure 1.3:</b> The optimized hydrogen bonded adduct of furan-water cluster showing classical (O-H•••O) and non-classical (O-H••• $\pi$ ) hydrogen bonding, Adapted from Kaur and co-workers [ ....	6
<b>Figure 2.1: Synthesis process of DFM.....</b>	<b>12</b>
<b>Figure 2.2:</b> Molecular structure of furan.....	19
<b>Figure 3.1:</b> Equilibrium structure of DFM (Global minimum) and the Equilibrium structure of DFM (showing numbering according to IUPAC) .....	24
<b>Figure 3.2:</b> Conformational structures of DFM molecule.....	27
<b>Figure 3.3:</b> Experimental and calculated proton NMR spectra for DFM molecule calculated at B3LYP/ 6-31+G(3d, 3p) .....	38
<b>Figure 3.4:</b> Experimental <sup>1</sup> H- NMR spectrum of DFM in CDCl <sub>3</sub> .....	40
<b>Figure 3.5:</b> $\sigma$ -type hydrogen bonding as calculated at B3LYP+G(3d,3p) level of theory.....	44
<b>Figure 3.6:</b> $\pi$ -type hydrogen bonding scheme as calculated at B3LYP+G 6-31(3d, 3p) level of theory .....	45
<b>Figure 3.7:</b> Molecular electrostatic potential map (MEP) OF DFM.....	46
<b>Figure 3.8:</b> Potential energy surface of Complex A.....	47
<b>Figure 3.9:</b> Relaxed energy scan profile .....	50

## ABSTRACT

*Ab Initio* Hatree-Fock (HF) and Density Functional Theory (DFT) are used to study the molecular structure of difurylmethane (DFM) and its interaction with methanol (MeOH) in the formation of DFM-MeOH complexes. The molecular structure of difurylmethane is further probed by using experimental proton nuclear magnetic resonance ( $^1\text{H-NMR}$ ), gauge including atomic orbital nuclear magnetic resonance (GIAO-NMR), Fourier transform infrared (FTIR) spectroscopy analysis to elucidate any structure-property relations which may play a role in the DFM-MeOH complex formation.

Conclusions from previous work in the researcher's laboratory on ultrasonic speeds and volumetric studies of mixtures of DFM and a series of ( $\text{C}_1\text{-C}_6$ )-n-alkanol binary solutions underpins dipole-dipole interactions and possibly hydrogen bonding as the main intermolecular forces between molecules in the solution. To probe this further a theoretical and experimental investigations on the system is required. The scope of this work is to study the interactive behavior of DFM-MeOH complex system through computational methods using relevant model chemistries.

The geometries of DFM molecular structures were optimized without symmetry constraints, using Gaussian '09 package with B3LYP / 6-31+G (3d, 3p) method. The nature of stationary point was evaluated using harmonic frequency analysis and it was confirmed to be a local minimum in the potential energy surface. The potential energy surface scanning tool (PESST) was used to generate 12 conformational structures of DFM, by varying the angle between two furanic rings at an increment of 30 degrees. The global minimum in the Potential Energy Surface is located when the oxygen atoms in the furan rings are as far away from each other as possible and on opposite sides. Results from experimental  $^1\text{H-NMR}$  and FTIR spectroscopy analysis of the DFM molecule agree with the molecular structure obtained from computational B3LYP/6-31+G(3d,3p) methodology

For the DFM-Methanol complexes, two equilibrium complexes were obtained and identified as either  $\sigma$ -type or  $\pi$ -type configurations where the  $-\text{OH}$  moiety of the methanol with the oxygen atom of the furan ring in the  $\sigma$ -type and the  $-\text{OH}$  interacts with the  $\pi$ -system of the furanic ring in the  $\pi$ -type configuration respectively. The basis set superposition error (BSSE) and thermal energy (calculated under the harmonic-rigid rotor approximation) corrected stabilization energies

associated with the  $\sigma$ -type and  $\pi$ -type configurations are -3.16 kcal / mol. and -1.89 kcal / mol. suggesting that the  $\sigma$ -type configuration is the most favorable interaction. In a different study Kgagodi and Mbaiwa did similar study on DFM-n-propanol binary mixture (employing Molecular Mechanics and *ab-initio* methods) looking at the thermodynamic properties and structure. The results obtained from radial distribution functions and ab-initio calculations show evidence of hydrogen bonding between n-propanol and DFM via the acidic hydrogen of -OH group in MeOH and the hetero atom of DFM which is agreement with conclusions from this study on the most probable interaction between DFM and R-OH.

# 1 INTRODUCTION

Forces of interaction that exist between molecular species often give rise to the formation of clusters and/or bulk phases. Studies of intermolecular interaction allow us to understand many phenomena in science such as the shapes and properties associated with biological and synthetic macromolecules [1]–[4]. The underlying difference in the nature of intermolecular interactions gives rise to disparity in physical properties in clusters and bulk phases e.g. the self–association of water molecules in a bulk phase that occurs through hydrogen bonding and also intra-molecular interactions (dipole-dipole interactions) of tertiary amines contributes to differences in viscosity, boiling point and solubility properties of these two systems. Some of these differences in properties such as in boiling points and solubility ratios occurring between different components in a solution mixture are utilized in separation science. They are used to augment the efficiency of separation of various components in solution mixtures such as in solvent extraction and distillation methods. Another example is found in processes involving chelating compounds which are the result of hydrogen bonding of different species binding together through two or more sites of one molecule to another. The implication of hydrogen bonding in biological systems ranges from the essence of protein folding to formation of DNA molecular structure. In the folding of proteins for example, hydrogen bonding can occur between the hydrogen of an amine and an electronegative element such as oxygen in another residue as a protein folds into place; in addition hydrogen bonds hold complementary strands of DNA together. [1]

In recent investigations in the writer’s research laboratory [5]–[7], experimental work (using ultrasonic speeds and density measurement) was done to study the nature of intermolecular forces that occur between difurylmethane (DFM) and ( $C_1$ - $C_6$ )-*n*-alkanol binary solutions [5], DFM with ( $C_5$ - $C_8$ )-*n*-alkanes (*n*-pentane, *n*-hexane, *n*-heptane, *n*-octane) [6] or amides (N-methylformamide, N-ethylformamide, N,N-dimethylformamide, N,N-dimethylacetamide) [7] over the entire composition range (0 to 1 in the mole fraction scale) at various temperatures. Thus thermodynamic properties such as volumetric changes were used to yield useful information about the system’s intermolecular interactions and its internal behaviour. These volumetric properties were found not to be additive (as in  $1+1 \neq 2$ ) and as such do not show ideal behaviour: Deviations from ideal behaviour are determined from thermodynamic parameters of solution mixtures such as excess molar volume, excess partial molar volume and limiting partial molar volume in the previous work [5]–[7] and elsewhere [8]–[11].

Difurylmethane (DFM) was first identified by Dunlop and co-workers [12], in 1953 as one of the products of furfuryl alcohol oligomerization. DFM has since found wide utility as an alternative substitute for diphenyl methane [13], [14]. DFM is an aprotic solvent and its molecular species self-associate through dipole-dipole interactions giving rise to a pure dipolar fluid [5], [6]. DFM is made of two furan rings linked by a methylene group as shown in Figure 1.1 below.

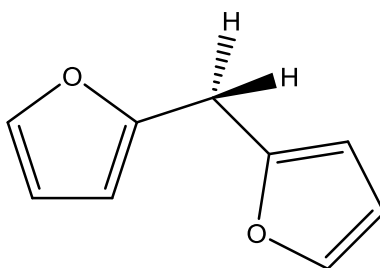


**Figure 1.1: Structure of difuryl methane**

Conclusions from previous work in the writer's research laboratory [5]–[7] on volumetric changes of a mixture of DFM and a series of (C<sub>1</sub>-C<sub>6</sub>)-n-alkanol binary solutions underpin dipole-dipole interaction and possibly hydrogen-bonding as the underlying intermolecular forces between molecules in the system. To probe this further a theoretical and an experimental investigation on the system is required.

## **1.1 Scope of the Study**

The scope of this work is to study the interactive behaviour of a DFM + methanol complex system through computational methods using relevant model chemistries. Hartree-Fock (HF) and Density Functional Theory (DFT) procedures are used in combination with 6-31+G (3d, 3p) basis set to characterize the DFM molecule and then DFM-Methanol complexes. The choice of the Model Chemistry (DFT or HF and associated basis sets and what they represent are explored and detailed under Section 2.2 Computational Methods). These computational calculations are used to determine the nature of intermolecular interactions within the DFM-Methanol complex. For the DFM molecule experimental Infra-Red (IR), proton nuclear magnetic resonance (<sup>1</sup>H-NMR) and computational work are compared to our own spectral calculations on DFM using Hartree-Fock and DFT methods. This will be discussed in detail under results and discussions.

In this study, preliminary investigations are done on a furan molecule, which is a structural moiety of DFM, in order to help us select the most appropriate model chemistry suitable for our work. There are several model chemistries used in the preliminary study of furan to decipher electronic structure properties such as dipole moment, equilibrium structure and polarizability. The model chemistries employed involve: B3LYP/ G(d), B3LYP/ 6-31+G(d,p) and B3LYP/ 6-31+G(3d,3p). There is extensive literature on the comparison between theoretical and experimental molecular structural properties of furan which gives a platform to decipher the most appropriate model chemistry to use for DFM. In the preliminary investigations Furan was first optimized to identify equilibrium structures with more computational work done to determine its net dipole moment and static polarizability and these are compared with experimental values where possible. Molecular parameters of the equilibrium structure of furan, such as bond lengths and bond angles are compared to literature values as well as the net dipole moment and static polarizability. The most efficient model chemistry (6-31+G(3d,3p)), for furan is then adopted for further work on DFM-Methanol following this investigation through a potential energy scan to obtain a global minimum representative isomer of DFM.

In the following section we explore intermolecular interactions in general and discuss a platform which focuses on the system of interest for the (DFM + MeOH) binary system.

## 1.2 Objectives

The objectives of this work is to study the structural parameters and properties of DFM and DFM-MeOH complexes. The nature of intermolecular interactions between the two monomers; DFM and MeOH will be interrogated using computational simulations.

## 1.3 Intermolecular Interactions

Intermolecular interactions are ubiquitous in virtually all areas of science. The hydrogen bond (X-H ··· A) in particular [15], [17], [18] is central to chemistry and biology. A hydrogen bond is an electrostatic attraction between two polar groups (one a donor and the other an acceptor) that occurs when a hydrogen (H) atom, bound to a highly electronegative atom such as nitrogen (N), oxygen (O), or fluorine (F), experiences the electrostatic field of another highly electronegative atom nearby [19].

Hydrogen bonds can occur between molecules (intermolecular) or within different parts of a single molecule (intramolecular). Depending on the nature of the donor and acceptor atoms which constitute the bond, their geometry, and environment, the energy of a hydrogen bond can vary between 1 and 40 kcal/mol. This makes the hydrogen bond somewhat stronger than a van der Waals interaction, and weaker than covalent or ionic bonds. This type of bond can occur in inorganic molecules such as water and in organic molecules like DNA and proteins. A comparison and classification and terminology of hydrogen bonds is shown in Figure 1.1 and Table 1.1 below



**Figure 1. 2: Schematic of Hydrogen bonding showing donor acceptor rearrangement**

**Table 1.1: Classification of Hydrogen Bonds [19]**

	Strong	Moderate	Weak
D-H...A	mostly covalent	mostly electrostatic	electrostatic
Bond lengths	D-H $\approx$ H...A	D-H < H...A	D-H $\ll$ H...A
H...A (Å)	1.2-1.5	1.5-2.2	2.2-3.2
D...A (Å)	2.2-2.5	2.5-3.2	3.2-4.0
Bond angles (°)	175-180	130-180	90-150
Bond energy (kcal mol <sup>-1</sup> )	14-40	4-15	<4
Examples	HF complexes acid salts proton sponges	Acids Alcohols Hydrates All bio-molecules	Gas phase dimers C-H...O/N O/N-H... $\pi$ CH... $\pi$

The importance of hydrogen bonding interactions in nature, such as O-H  $\cdots$   $\pi$ , C-H  $\cdots$  O, C-H  $\cdots$   $\pi$ , and N-H  $\cdots$   $\pi$ , have been identified [20]. There are two categories of intermolecular hydrogen bonding types namely classical and non-classical hydrogen bonding. The classical hydrogen bonding involves the F, O, N atoms within the bonding fragments i.e. O-H  $\cdots$  O, O-H  $\cdots$  F and O-H  $\cdots$  N. In contrast the non-classical hydrogen bonding type may involve one species not being



one of the N, O and F atoms i.e. O-H $\cdots\pi$ , C-H $\cdots$ O, C-H $\cdots\pi$ , and N-H $\cdots\pi$  bonds [21]. Previous experimental and computational studies have been undertaken in the areas of classical and non-classical hydrogen bonding in a vast number of systems. In non-classical H-bonding the interaction scheme of the type O-H $\cdots\pi$  has received widespread attention [22]–[28]. Kaur and co-workers [29] did a study on heterocyclic-water adducts e.g. the furan-water adduct was examined and essentially classified as an example of a system that interacts through both types of hydrogen bonding schemes. In general two types of hydrogen bonding scheme within the furan-water cluster was established and it is of the following type: O-H $\cdots\pi$  and O-H $\cdots$ O [11], [15]–[17]. It was observed that the O-H $\cdots$ O configuration is the global minimum due to the presence of contracted lone pairs as opposed to highly delocalized electrons in  $\pi$ -cloud around the furanic ring system. In the O-H $\cdots\pi$  bonding type, a proton of the O-H group points directly to the site of  $\beta$ -carbon of furan ring [21], [29]–[31].

Other investigations on the nature of intermolecular interaction present in heterocyclic (such as furanic-water) systems sought to address the following research questions

- 1.2.1 Molecular structural parameters (bond length and bond angles);
- 1.2.2 Binding energies (BE<sub>s</sub>) between molecules;
- 1.2.3 Molecular vibrations via infrared spectroscopy;
- 1.2.4 Natural bond orbital (NBO) analysis ;
- 1.2.5 Molecular electrostatic potential (MEP) maps which give insight into the nature of the interactions of pyridine, furan and thiophene with LiNH<sub>3</sub> [30] and
- 1.2.6 Bader's atom in a molecule (AIM) analysis was employed in a study of Benzene (B)-Water (W), BZW<sub>n</sub> (n=1-10) clusters [20].
- 1.2.7 Molecular mechanics and ab-initio study of DFM-n-propanol

These are explored in detail as follows:

### 1.3.1 Molecular Structural Parameters

The study of intermolecular bond distances often provides essential information about the nature of hydrogen bonding and changes in structural parameters of the individual molecules in the cluster

due to complex formation. In the area of structural parameters Kaur and co-workers [29] looked into  $r(\text{O}-\text{H}\cdots\pi)$  and  $r(\text{O}-\text{H}\cdots\text{O})$  bond distances in a furan-water cluster (see Figure 1.2 below).

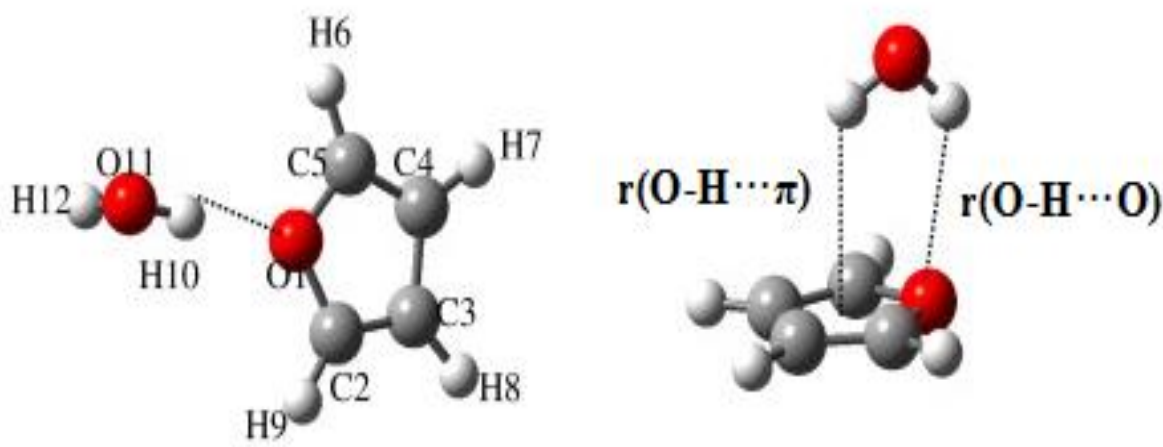


**Figure 1.3: The optimized hydrogen bonded adduct of furan-water cluster showing classical ( $\text{O}-\text{H}\cdots\text{O}$ ) and non-classical ( $\text{O}-\text{H}\cdots\pi$ ) hydrogen bonding, Adapted from Kaur and co-workers [29]**

It was established that the classical hydrogen bonding  $\text{O}-\text{H}\cdots\text{O}$  is the predominant configuration of the two bonding schemes. The intermolecular distances  $r(\text{C}-\text{H}\cdots\text{O})$ ,  $r(\text{O}-\text{H}\cdots\pi)$  and  $r(\text{O}-\text{H}\cdots\text{O})$  agree well with the experimental values [31]. In general hydrogen bonding is obtained when the intermolecular bond distance is less than the Van der Waals atomic radii of the two binding fragments. Furthermore the classical hydrogen bonding scheme features a much smaller intermolecular bond distance that is less than the bond distance associated with the non-classical hydrogen bonding scheme and thus molecular geometry is a useful feature in the classification of hydrogen bonding [31].

### 1.3.2 Binding Energies

Binding energies ( $\text{BE}_s$ ) have profound implications in classification of hydrogen bonds [16]. Since different types of hydrogen bonding configurations (classical and non-classical bonds) are associated with unique values of stabilization or binding energies. Binding energies ( $\text{BE}'\text{s}$ ) are calculated and corrected for basis set superposition error (BSSE) and zero point vibrational energy (ZPE). The BSSE calculations are done in this work.

The Boys and Bernadi counterpoise correction (CP) procedure was employed to remove BSSE [32]. The uncorrected interaction energies between monomer A (DFM) and monomer B (MeOH) were calculated as:

$$\Delta E_{\text{int}}(AB) = E_{AB}^{AB}(AB) - E_A^A(A) - E_B^B(B) \quad (1.1)$$

Where the superscripts denote the basis used the subscripts denotes the geometry and the symbol in brackets denote the chemical structure considered.

THUS ,  $E_{AB}^{AB}(AB)$  represents the dimeric complex AB (DFM-MeOH) evaluated in the dimer basis sets. Likewise , monomers A and B were evaluated at their own geometries and basis. The correction to BSSE was evaluated as:

$$E_{\text{BSSE}}(A) = E_A^{AB}(B) - E_A^A(A) \quad (1.2)$$

$$E_{\text{BSSE}}(B) = E_B^{AB}(B) - E_B^B(B) \quad (1.3)$$

The energy of monomer A in its monomer basis is substituted from energy of monomer A in the dimer basis (and likewise for monomer B) [32].

The Boys and Bernadi counterpoise correction is calculated as:

$$\Delta E_{\text{int}}^{\text{CP}}(AB) = E_{AB}^{AB} - E_A^{AB} - E_B^{AB} \quad (1.4)$$

A study done by Daiqian [31] compared the energy of geometries between two structures (A) and (B) where structure (A) is Cl-H...O and structure (B) is Cl-H... $\pi$  which are both formed through a non-classical hydrogen bonding to a heteroatom and a  $\pi$ -system. The energy profiles of both structures show that structure (A) corresponds to a global minimum. There is a strong correlation between the binding energy BE (O...H) and the distance  $r(\text{O}\cdots\text{H})$  than to BE ( $\pi\cdots\text{H}$ ) and  $r(\pi\cdots\text{H})$ , since the lone pair electrons in the O are more contracted (localized) than  $\pi$  electrons. The results show that the interaction of Cl-H...O is stronger than that of Cl-H... $\pi$ .

### 1.3.3 Molecular Vibrations / Infrared Spectral Analysis

The nature of hydrogen bonding (classical or non-classical) can be studied using infrared (IR) spectral analysis. In theory, due to the nature of interaction of hydrogen acceptor-hydrogen donor

atoms, X-H · · · Y (where Y is hydrogen acceptor atom and X-H is hydrogen donor group), the r(X-H) bond distance can either elongate or shorten during complexation. This change in r(X-H) bond distance can result in either red shift (r(X-H) bond elongation) or blue shift (r(X-H) bond contraction) in vibrational frequency. By studying the extent of IR frequency shift and change in peak intensity we can successfully classify the type of intermolecular bonding scheme into either classical or non-classical hydrogen bonding. In all of the optimized X-H · · · Furan (where X= O, N, Cl or F), the X-H bond length is elongated and its vibrational frequency is red shifted with subsequent increase in intensity. This behaviour is somewhat similar to that observed in spectral analysis of conventional hydrogen bonding schemes; for example X-H · · · Furan (where X= O, N or F). In a study conducted by Xie and co-workers [31] on the nature of intermolecular interactions within HCl-Furan complex, it was uncovered that the change in H-Cl vibrational frequency is negative (thus the measured H-Cl frequency after complexation is smaller than the frequency of free fragment) - indicative of the ongoing red shift [30], [31], [33]–[37].

### 1.3.4 Natural Bond Orbital (NBO) Analysis

Another method of studying hydrogen bonding is the Natural Bond Orbital (NBO) analysis; whereby the hydrogen bond acceptor abilities of heteroatom and the  $\pi$ -electron cloud of the ring are compared. The NBO analysis was used to study the furan-water complex [29]. The energy gap between HOMO (furan) and LUMO (water) determines the overlapping strength between these two frontier orbitals. Thus in the NBO analysis we can mention two types of hydrogen bonding interactive schemes, namely  $\sigma$ -type (O-H · · · O) and  $\pi$ -type (O-H · · ·  $\pi$ ) hydrogen bonding. In the first configuration ( $\sigma$ -type) there is a hydrogen bond transfer from donor orbital ( $\sigma^*$  or O-H<sub>water</sub>) towards heteroatom (O, lone pair) acceptor orbital whereas the second configuration involves hydrogen bond transfer towards the  $\beta$ -carbon of the ring. The magnitude of overlap between bonding NBO and anti-bonding NBO frontier orbitals can be measured using second order perturbation energy. The second order stabilization (Perturbation) energy, ( $E^2$ ) is associated with electron delocalization for instance in the case of furan from n (lone-pair)  $\rightarrow \pi^*$  or  $\pi \rightarrow \pi^*$ .  $E^2$  is represented by the equation:

$$E^2 = -2(F_{ij}/\Delta E_{ij}) \quad (1.5)$$

Where  $\Delta E_{ij} = E_i - E_j$  is the difference in energy between the interacting molecular orbitals  $i$  and  $j$ ,  $F_{ij}$  is the Fock matrix elements for the interaction between orbitals  $i$  and  $j$ .

In a system involving hydrogen bonding between furan and methanol, which is somewhat similar to the system involving difurylmethane-methanol which is under investigation for this study, there are two types of interactive schemes ( $\sigma$ -type (O-H $\cdots$ O) and  $\pi$ -type (O-H $\cdots\pi$ )) also known as classical and non-classical hydrogen bonding schemes. The  $\sigma$ -type occurs at the lone pair site of the hetero atom (which is Oxygen) but the  $\pi$ -type configuration occurs at  $\beta$ -carbon of the furanic ring. Using the computed magnitude of second order perturbation energy done by various workers, [29]–[31] it is noted that the classical hydrogen bonding or the  $\sigma$ -type configuration is the most stable energy structure compared to non-classical or the  $\pi$ -type configuration [29]–[31] and this hypothesized to be similar in the DFM-MeOH complex under study herein.

### 1.3.5 Molecular electrostatic potential (MEP) map

Molecular electrostatic potential (MEP) map is an important tool in exploring the nature of intermolecular interactions. Hua Yan and co-workers [30] did a plot of 3-dimensional MEP map around furan ring to estimate its bonding aspects with relevant molecular structure while working with furan- LiNH<sub>2</sub> complex.

From this map (furan) of potential energy surface, it was elucidated that both the immediate vicinity of the O atom and the region above the ring show noticeable negative electrostatic potential thus resulting in two generic configuration schemes for Furan-X dimer (where X= hydrogen bond donor molecule) [30]. The potential site of hydrogen bonding in furanic rings giving rise to the most stable complex as elucidated by MEP is in agreement with that suggested by Molecular Structural Parameters, Natural Bond Orbital (NBO) Analysis, and Binding Energies as discussed in Sections 1.2.1, 1.2.2 and 1.2.4 above respectively.

### 1.3.6 AIM Analysis

The atom in a molecule (AIM) analysis is a useful tool to measure the hydrogen bonding using the calculated electron densities and Laplacian [23], [29] Similar studies to those done on furan-X

(elucidating the nature of intermolecular forces) were conducted on benzene(B)-Water(W) (BZW<sub>n</sub> (n=1-10) ) [21] by surveying the geometries, BEs, IR spectroscopy and AIM analysis of the complexes. The AIM analysis somehow revealed three types of bonding schemes in BZW<sub>n</sub> (n=1-10) clusters; O-H... $\pi$  cloud, C-H...O (W) and O-H...O (furan), and evidence of red shift in the O-H stretching frequency

### 1.3.7 Molecular Mechanics (MM) and Ab-initio study of DFM-n-propanol

In a different study Kgagodi and Mbaiwa [30] have investigated the DFM-n-propanol binary mixture using Molecular Mechanics simulations to look at the thermodynamic properties and structure of the system. The data obtained from radial distribution functions and ab-initio calculations show evidence of hydrogen bonding between n-propanol and DFM via the acidic hydrogen atom of -OH group and the hetero atom (Oxygen) of DFM. The results reported for DFM-n-propanol complex are in agreement with the results reported herein (vide infra) for DFM-MeOH complex employing Density Functional Theory calculations.

## 2 METHODOLOGIES

### 2.1 EXPERIMENTAL METHODS

#### 2.1.1 Materials and purification of solvents

For experimental work, the following chemicals were used: acetone (Skylabs chemicals, analytical reagent, 99%), acetonitrile (E-lab Direst Limited chemicals, spectral reagent, 99.5%), ammonia solution (Rochelle chemicals, 25%), furan (Merck Co., 99.0%), furfuryl alcohol (Merck Co., 98.0%), borontrifluoridedietherate catalyst (Sigma-Aldrich Chemicals Co., 99.0%), sodium hydroxide pellets (Rochelle Chemicals, 99.0%), anhydrous sodium carbonate (Glassworld, analytical reagent, 99.5%), ethanol (Sigma-Aldrich Chemicals, 99.5%), molecular sieves (Sigma-Aldrich).

#### 2.1.2 Purification of solvents

**Acetonitrile:** This solvent was purified by distillation using 1 metre fractionation column fitted with glass beads. The purified Acetonitrile was then stored in tightly stoppered bottles to prevent atmospheric contamination.

**Ultrapure water:** Distilled water was first de-ionized by means of ion exchange resins, then refluxed over  $\text{KMnO}_4$  and finally doubly distilled under nitrogen flow using a two-stage Heraeus Destamat quartz still instrument. Its conductivity was always less than  $1.0 \times 10^{-6} \text{ S-cm}^{-1}$ .

### 2.1.3 Preparation of the difurylmethane (DFM)

Difurylmethane (DFM) was prepared in accordance to the modified method from the literature [38]. Acetonitrile was first distilled before preparation of the reaction mixture. To minimize the self-polymerization of furfuryl alcohol, which would result in lower DFM yield and to enhance its coupling to furan, the initial molar ratio of furfuryl alcohol to furan in the reaction mixture was kept low at (1:10). Furan ( $400 \text{ cm}^3$ , 5.46 mol), and boron trifluoride dietherate catalyst ( $0.40 \text{ cm}^3$ ,  $3.28 \times 10^{-3} \text{ mol}$ ) were dissolved in acetonitrile solvent ( $300 \text{ cm}^3$ ) in a  $3 \text{ dm}^3$  round bottom flask. Furfuryl alcohol ( $40 \text{ cm}^3$ , 0.46 mol) was dissolved in acetonitrile ( $300 \text{ cm}^3$ ), and thereafter the solution was added drop-wise to a stirred (furan +  $\text{BF}_3(\text{OEt}_2)_2$ ) mixture at room temperature. In the first 80 minutes, the colour of the reaction mixture intensified from light yellow to an intermediate dark green and finally to dark brown. The reaction mixture was allowed to stand overnight at room temperature while being continuously stirred to ensure homogeneity: high conversion of furan to difurylmethane (DFM). The reaction occurs according to the following scheme:

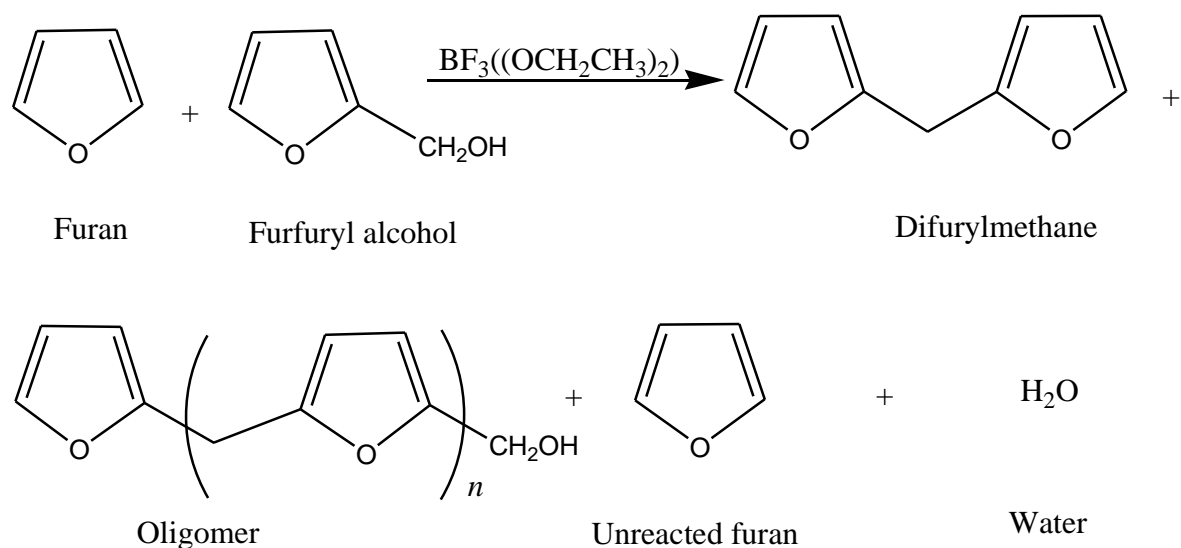


**Figure 2.1: Synthesis process of DFM**

At the end of a 12h reaction time, 25cm<sup>3</sup> of 5% aqueous ammonia was added to neutralize boron trifluoride dietherate catalyst. The reaction mixture turned from deep brown to a light yellow colour as an indication of reduction of polymerization rate of alcohol. The un-reacted furan and acetonitrile solvent were evaporated from the reaction mixture by a means of a rotary evaporator. The reaction products were then dissolved in 150 cm<sup>3</sup> acetone to form a light brown clear solution. Whereas DFM has a very high solubility in *n*-hexane, the unreacted furfuryl alcohol, its oligomers and other by-products such as water show very poor solubility. At this point we took advantage of the high solubility of DFM in *n*-hexane to separate it from the reaction products. The reaction products now dissolved in acetone were poured into 500 cm<sup>3</sup> of vigorously stirred *n*-hexane and the light yellow *n*-hexane phase was filtered off, *n*-Hexane and acetone were evaporated off. The remaining impure DFM was re-dissolved in 300 cm<sup>3</sup> fresh *n*-hexane. The solution was then extracted with 100 cm<sup>3</sup> portions of 1M aq. NaOH. The extraction was continued until the aqueous phase remained colourless. The *n*-hexane phase was washed with dil. NaOH followed by several portions of water to remove NaOH, and thereafter dried over several portions of baked Na<sub>2</sub>CO<sub>3</sub>. The solvent was distilled off with a rotary evaporator giving a DFM yield of 70 to 85% on the furfuryl alcohol basis. DFM was



further purified by distillation under partial vacuum and its purity confirmed by  $^1\text{H-NMR}$  and elemental analysis. When freshly purified, DFM is a light yellow liquid. Like many furan compounds, DFM slowly darkens in colour over several days due to photo-decomposition. Storage of DFM in a dark-brown bottle covered by aluminum foil partly prevents the deterioration of its colour.

#### **2.1.4 Sample preparation for NMR Analysis**

Sample preparation for NMR involves a mixture of few drops of DFM with chloroform which was then run on Bruker Advance DPX 300 MHz to obtain  $^1\text{H-NMR}$  spectra for DFM using  $\text{CDCl}_3$  as a solvent, 99.8 % supplied by Aldrich. All the spectra were recorded at room temperature with all chemical shifts recorded against a reference peak of internal standard, Tetramethyl silane (TMS).

#### **2.1.5 Sample preparation for IR spectral analysis**

Few drops of DFM were smeared on FTIR spectrometer sample crystal and an IR spectrum was recorded using Perkin Elmer HATR spectrum 2 FTIR spectrometer

### **2.2 COMPUTATIONAL METHODS**

Computational calculations on Furan and DFM were undertaken in gas phase using Hartree-Fock (HF) and Density Functional Theory (DFT) theoretical methods run on the Gaussian '09 suite of program using 6-31+G (3d,3p) basis set: Each method is briefly outlined as follows.

#### **2.2.1 Hartree-Fock (HF)**

We are interested in describing electronic charge distribution in molecules. Electrons are small and very nimble and they move very fast and nuclear positions are considered to be parametric; when invoking the Born-Oppenheimer approximation. Electronic structure of molecular species can only be described using quantum mechanics. Molecular wave functions were initially described using Hartree Product in the literature (equation 2.2). Molecular wave functions are now accurately described using linear combinations of atomic orbitals. These atomic orbitals are depicted as single Slater determinants because electrons are fermions and thus there is a need to

enforce anti-symmetry principle (see equation 2.3) in electrons (the wave function of electrons change sign when we exchange positions of the two electrons) in order to capture the accurate description of electron distribution. The many body Schrödinger equation (equation 2.1) cannot be solved exactly and hence approximation models are invoked. Hartree-Fock approximation model is one of the methods that can be used to solve Schrödinger equation.

$$H\Psi = E\Psi \quad (2.1)$$

Above is a time independent Schrödinger equation, where H is the Hamiltonian,  $\Psi$  is the wave function, and E is the Eigen value (energy) of the time independent Schrödinger. Hartree-Fock is an ab-initio technique and usually gives a crude approximation solution to the problems solved. It is the basis of molecular Orbital (MO) theory: electrons are described by a single particle function; thus ignoring electron correlation effects.

$$\Psi_{\text{HP}}(r_1, r_2, \dots, r_n) = \Phi_1(r_1) \Phi_2(r_2) \dots \Phi_n(r_n) \quad (2.2)$$

$$\Psi(x_1, x_2) = \frac{1}{\sqrt{2}} Z(v) = \frac{1}{\sqrt{2!}} Z(v) = \frac{1}{\sqrt{2!}} [X_1(x_1) + X_2(x_2)] \quad (2.3)$$

$$\Psi(x_1, x_2) = \frac{1}{\sqrt{2!}} \frac{1}{\sqrt{2!}} \begin{vmatrix} X_1(x_1) & X_2(x_1) \\ X_1(x_2) & X_2(x_2) \end{vmatrix} \quad (2.4)$$

The equation depicted in 2.4 is the single Slater matrix of two electrons,  $X_i$  is a spin orbital wave function and  $x_i$  is electronic coordinates.

The Hartree-Fock procedure as an ab-initio method requires the use of a trial wave function whereby the solutions to Schrödinger equation are solved by a self-consistent approach. Hartree-Fock bears few advantages over other conventional computational methods like MP2 and coupled cluster(CC) since it requires less computer time to perform calculations in big systems and yields good results for barrier heights [39], [40] but does poorly in systems where electron correlations are important. When solving the Hartree-Fock equation; the self-consistent wave function is

optimized by minimizing the energy with respect to a trial wave function using a variational principle. Then the Fock operators (F) are obtained in the process, which involve the one electron operator term, interaction coulomb operator and exchange term and is the pseudo eigen value ( $\epsilon$ ).

$$F X (1) = \epsilon X \Phi (1) \tag{2.5}$$

### 2.2.2 Density Functional Theory (DFT)

Density functional theory employs the use of ground state density instead of wave-functions and it has resulted in reduced complexity of the computational time cost, because only 3 dimensional coordinates are required. Hohenberg and Kohn provided a proof in principle that the total energy used could be obtained from the ground state density [41], [42]. Kohn-Sham equation is depicted below:

$$\langle \Phi | H | \Phi \rangle = \int p(r)V(r)dr + F_{HK}[P(r)] = E[ P'(r) ] \geq E[ P_0(r) ] \tag{2.6}$$

$$F_{HK}[P(r)] = T[p] + V_{ee} [p] \tag{2.7}$$

$\int p(r)V(r)dr$  ..... External potential  
 $T[p]$  ..... Kinetic energy  
 $V_{ee} [p]$  ..... Inter-electronic potential

The solutions for  $T[p]$  and  $V_{ee} [p]$  are not known.

The practical application of DFT became apparent in 1965 when Kohn –Sham provided a plausible solution for the kinetic energy term by using single–electron orbitals.

$$\left( \frac{1}{2} \nabla^2 + V (r) + \int \frac{p'(r')}{|r-r'|} dr' + V_{xc} \right) \Phi_i = E \Phi_i \tag{2.8}$$

Where:

$V(r)$ : Electron-nuclear electrostatic potential

$\rho(r)$ : Electron density

$r$ : electronic distance from the nucleus

$V_{xc}$ : Exchange-correlation term

The exchange-correlation term  $V_{xc}$ , is still enigmatic and can only be approximated. Since electronic correlation, exchange and kinetic terms pose great difficulty in general solutions of Schrödinger equation correction factor known as correlation-exchange functional are embedded in the Kohn-Sham equation as an error correction terms. The exchange-correlation term ( $V_{xc}$ ) is still enigmatic and can only be approximated. Computational chemists have devised a number of exchange-correlation functional terms optimized for DFT calculations of different electronic structure properties

In this work the functional adopted is B3LYP: Consisting of Becke-3 parameter exchange term and LYP correlation functional. This functional relatively yields excellent results for energy, barrier heights and harmonic vibrational frequencies much better than most existing functionals, however even though DFT shows excellent results when used with a good functional, it should not be used for studying ionic compounds due to its general poor performance in calculations involving ionization energies. In terms of computational cost DFT is comparable to Hartree-Fock but gives excellent results somewhat equivalent to correlated methods such as  $MP_2$  [43]–[47]. In this work we employ both HF and DFT (B3LYP) to characterize molecular structures and properties such as dipole moment and polarizability for Furan and DFM and for Energy of complexation between DFM and Methanol.

### **2.2.3 The Formulation of Basis Sets**

A basis set is a set of functions used to create molecular orbitals, which are expanded as a linear combination of atomic orbitals with coefficients as variational parameters to be determined. In the early days of quantum chemistry, the so-called Slater type orbitals (STOs,) were used as basis functions due to their similarity with the Eigen functions of the hydrogen atom. STOs have an advantage in that they have direct physical interpretation and thus are naturally good basis for molecular orbitals. However, from a computational point of view the STOs have the severe

shortcoming that most of the required integrals needed in the procedure must be calculated numerically which drastically decreases the speed of a computation.

STOs can be approximated as linear combinations of Gaussian orbitals. Gaussian Type Orbitals (GTOs) are not really orbitals. They are simpler functions and are frequently called Gaussian primitives. The smallest possible basis set is called the minimal basis set, and it contains one orbital (which may be contracted) for every orbital we usually think of an atom (including unoccupied orbitals). For example, hydrogen has just one orbital, but carbon has 5 (1s, 2s, 2px, 2py, and 2pz) even though one of the p orbitals for carbon atom will be unoccupied. The STO-3G basis is a very well-known minimal basis set which contracts 3 Gaussian functions to approximate the more accurate (but more difficult to compute) Slater type orbitals. Although a contracted GTO might give a good approximation to an atomic orbital, it lacks any flexibility to expand or shrink in the presence of other atoms in a molecule. Hence, a minimal basis set such as STO-3G is not capable of giving highly accurate results.

The solution is to add extra basis functions beyond the minimum number required to describe each atom. Then, the Hartree-Fock procedure (Section 2.2.1) can weight each atomic orbital basis function more or less to get a better description of the wave function. If we have twice as many basis functions as in a minimum basis, this is called a "double zeta" basis set (the zeta, comes from the exponent in the GTO). Hence, a double-zeta basis set for hydrogen would have two functions, and a true double-zeta basis set for carbon would have 10 functions. However, sometimes Computational Scientists use only a single orbital for the core (1s), giving 9 functions for carbon. Such basis sets are said to be "double-zeta in the valence" space; they are also called "split-valence" basis sets. Double-zeta basis sets are often denoted DZ. Often additional flexibility is built in by adding higher-angular momentum basis functions. Since the highest angular momentum orbital for carbon is a p orbital, the "polarization" of the atom can be described by adding a set of d functions.

The late Nobel Laureate, John Pople developed a basis set notation, which was subsequently popularized by the Gaussian set of programs as follows.

- STO-3G is a minimal basis set in which each AO is represented by 3 Gaussians (3G), chosen to mimic the behaviour of a STO.

- Pople's split-valence double-zeta basis set is called 6-31G; the core orbital is a CGTO made of 6 Gaussians, and the valence is described by two orbitals — one CGTO made of 3 Gaussians, and one single Gaussian in the valence orbitals.
- 6-31G\* [or 6-31G(d)] is 6-31G with added d polarization functions on non-hydrogen atoms; 6-31G\*\* [or 6-31G(d,p)] is 6-31G\* plus p polarization functions for hydrogen
- 6-311G is a split-valence triple-zeta basis; it adds one GTO to 6-31G
- 6-31+G is 6-31G and diffuse s and p functions for non-hydrogen atoms; 6-31++G has diffuse functions for hydrogen also.

In this study, the choice of basis sets is premised on the above discussions as well as the results of several computational literature papers on the furan molecule which is the building block for the DFM molecule under study herein.

## 2.2.4 Equilibrium structures

Unlike DFM the amount of theoretical calculations done on furan is very extensive. Several ab-initio and DFT calculations on furan is about its equilibrium structure, dipole moment, harmonic frequencies and many other fundamental molecular properties exist in the literature. And since DFM is a molecular derivative of furan, we can assume that most of electronic structure properties associated with furan are also common to DFM. We therefore select furan as a prototype molecule to conduct preliminary investigations so that we are able to determine appropriate theoretical model and basis set suitable for the calculations we need to perform on DFM.

Baldrige and co-workers [48], [49] calculated molecular structures of 5-membered heterocyclic molecules including furan using HF/ 3-21G(d). The results of these calculations together with other literature values are shown in Table 2.0 with the corresponding calculated (HF/ 3-21G(d)) geometric parameters; such as bond lengths and bond angles had average deviation of 1.34 and 3.21% respectively from the experimental values [42], [50], [51]; thus making the calculated (HF/3-21G(d)) values for furan to have close resemblance to available literature values. These findings (calculated and experimental) correlate well with those we obtained using B3LYP/ 6-31+G(3d,3p). The structural parameters we computed for Furan show average deviation of 0.14 and 0.50 % in bond distance and bond angles respectively. The literature data on structural

parameters as depicted in Tables 2.1 to 2.3 show that lower theoretical models and basis sets have poor correlation with experimental values whilst higher models operating on sufficient basis sets have excellent agreement with available experimental values on equilibrium parameters. This is the basis for the selection of the model chemistry: B3LYP/ 6-31+G(3d,3p) in this work, as it performs on par with advanced model chemistries [52]–[57].

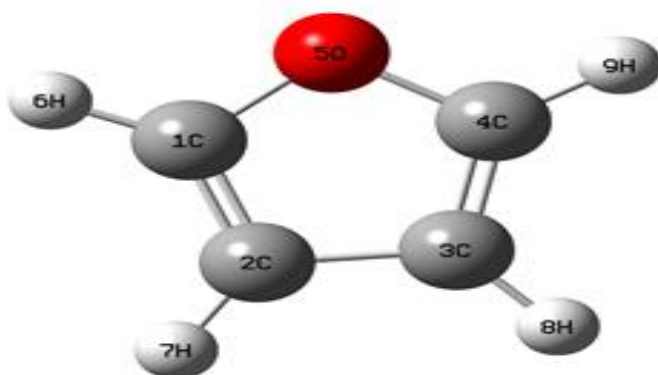


Figure 2.2: Molecular structure of furan

Table 2.1: Experimental (measured using microwave spectroscopy) and theoretical equilibrium structure for Furan bond lengths in angstroms optimized at different levels of theory and basis sets (in Å). Calculations in this work were performed using B3LYP/6-31+ (3d, 3p)

Method	$r(\text{C}_1\text{-O}_5)$	$r(\text{C}_1=\text{C}_2)$	$r(\text{C}_2\text{-C}_3)$	$r(\text{C}_4\text{-H}_9)$	$r(\text{C}_3\text{-H}_8)$
This work (B3LYP/6-31 +G (3d, 3p).)	1.364	1.3606	1.4354	1.0778	1.0793
HF/ 3-21G(d)	1.380 <sup>a</sup>	1.339 <sup>a</sup>	1.450 <sup>a</sup>	.....	1.065 <sup>a</sup>
B3LYP(sadlej-pol)	1.362 <sup>b</sup>	1.366 <sup>b</sup>	1.439 <sup>b</sup>	1.085 <sup>b</sup>	1.087 <sup>b</sup>
HF(sadlej-pol)	1.342 <sup>b</sup>	1.343 <sup>b</sup>	1.443 <sup>b</sup>	1.074 <sup>b</sup>	1.076 <sup>b</sup>
HF/ 6-31G(d,p)	1.344 <sup>c</sup>	1.3391 <sup>c</sup>	1.4406 <sup>c</sup>	1.0684 <sup>c</sup>	1.0703 <sup>c</sup>
<b>Experimental</b>	<b>1.362<sup>d</sup></b>	<b>1.3609<sup>d</sup></b>	<b>1.4309<sup>d</sup></b>	<b>1.0750<sup>d</sup></b>	<b>1.0768<sup>d</sup></b>
% deviation, this work to experimental values	0.15	0.022	0.32	0.26	0.23

<sup>a</sup>Reference [48], <sup>b</sup>Reference [52], <sup>c</sup>Reference [55], <sup>d</sup>Reference [50]

**Notes: Percentage deviation of theoretical calculations in this work to experimental values show that the chosen model chemistry in this work compares well with experimental values.**

### **2.2.5 Polarizability and dipole moment**

High angular momentum diffuse and polarized basis sets are able to describe the region of charge distribution accurately, thus they can be used in the calculation of dipole moments and high rank tensors such as static polarizability and hyper polarizability [52]. Alparone and coworkers [52] did work on polarizability calculations for chalcogenophenes ( $C_4H_4X$  ( $X= O, S, Se, Te$ )) using extended basis sets specifically designed for this type of calculations. Their data show that HF/HF/Pol method gives a poor estimate of the static polarizability with inherent percentage deviation from experimental data varying from 5% - 10 %. But when correlated geometries are used (HF//B3LYP/ Pol) the error is significantly reduced to  $\approx 2.3\%$ . The results of the work by Alparone *et al.* [52] closely resemble calculations in this work done at B3LYP/ 6-31+G (3d, 3p) theoretical level, showing small percentage deviation of 0.81% (for mean static polarizability) from the experimental value. These findings ascertain us that a smaller percentage discrepancy is measured, when correlated methods are employed [52], [58]–[61].

From the work done by Alparone and co-workers [52] using two diffuse and polarized basis sets, it can be shown that B3LYP/Pol gives the most accurate results that also correlates well with our findings in calculations of mean polarizabilities as depicted in Table 2.4.

Higher angular momentum and diffuse basis sets when combined with correlated methods yield excellent results in dipole moment and higher rank tensors – these findings are depicted in Tables 2.4 and 2.5 they somewhat agree with values obtained from experiment and the chosen model chemistry in this work [52], [58], [62], [63].



**Table 2.2: Experimental (measured using microwave spectroscopy) and theoretical equilibrium structure for Furan bond angles optimized at different levels of theory and basis sets in degrees ( $\theta$ ). Calculations in this work were performed using B3LYP/6-31+(3d,3p).**

Method	$\theta$ (C <sub>1</sub> -O <sub>5</sub> -C <sub>4</sub> )	$\theta$ (C <sub>3</sub> =C <sub>4</sub> -O <sub>5</sub> )	$\theta$ (O <sub>5</sub> -C <sub>4</sub> -H <sub>9</sub> )	$\theta$ (C <sub>2</sub> -C <sub>3</sub> =C <sub>4</sub> )	$\theta$ (C <sub>4</sub> =C <sub>3</sub> -H <sub>8</sub> )
This work (B3LYP/ 6-31+G (3d,3p))	106.889	110.413	115.881	106.143	127.461
HF/ 3-21G(d)	107.0 <sup>a</sup>	109.5 <sup>a</sup>	110.7 <sup>a</sup>	116.5 <sup>a</sup>	126.6 <sup>a</sup>
B3lyp(sadlej-pol)	107.1 <sup>b</sup>	110.5 <sup>b</sup>	106.5 <sup>b</sup>	133.2 <sup>b</sup>	126.4 <sup>b</sup>
HF(sadlej-pol)	107.2 <sup>b</sup>	110.9 <sup>b</sup>	105.5 <sup>b</sup>	132.4 <sup>b</sup>	126.4 <sup>b</sup>
HF/ 6-31 G(d,p)	107.1 <sup>c</sup>	110.8 <sup>c</sup>	116.3 <sup>c</sup>	105.6 <sup>c</sup>	125.6 <sup>c</sup>
<b>Exp</b>	<b>106.33<sup>d</sup></b>	<b>110.41<sup>d</sup></b>	<b>115.55<sup>d</sup></b>	<b>106.30<sup>d</sup></b>	<b>125.57<sup>d</sup></b>
% deviation, this work to experimental values	0.52	0.003	0.29	0.15	1.51

<sup>a</sup>Reference [48], <sup>b</sup>Reference [52], <sup>c</sup>Reference [55], <sup>d</sup>Reference [50]

**Notes:** Percentage deviation of the theoretical calculations used in this work to experimental values show that the chosen model chemistry in this work compares well with experimental values.

**Table 2.3: Equilibrium geometry and dipole moment for furan calculated at different levels of theory with 6-31G\*\* basis set**

Coordinate	Exp	HF	MP2 Full	MP2 Fc	DFT BLYP	DFT B3LYP	DFT LDA	DFT BVWN
O <sub>1</sub> -C <sub>2</sub>	<b>1.362<sup>a</sup></b>	1.343	1.364	1.366	1.382	1.364	1.351	1.383
C <sub>2</sub> =C <sub>3</sub>	<b>1.361<sup>a</sup></b>	1.339	1.365	1.366	1.371	1.361	1.361	1.369
C <sub>3</sub> -C <sub>4</sub>	<b>1.431<sup>a</sup></b>	1.441	1.426	1.427	1.444	1.435	1.422	1.443
C <sub>2</sub> -H <sub>6</sub>	<b>1.075<sup>a</sup></b>	1.069	1.074	1.075	1.086	1.079	1.088	1.080
C <sub>3</sub> -H <sub>7</sub>	<b>1.077<sup>a</sup></b>	1.070	1.075	1.076	1.087	1.080	1.089	1.082
C <sub>5</sub> -O <sub>1</sub> -C <sub>2</sub>	<b>1.06.5<sup>a</sup></b>	1.07.2	106.6	106.6	106.4	106.8	107.2	106.3
O <sub>1</sub> -C <sub>2</sub> -C <sub>3</sub>	<b>110.7<sup>a</sup></b>	110.8	110.5	110.5	110.5	110.5	110.4	110.5
C <sub>2</sub> -C <sub>3</sub> -C <sub>4</sub>	<b>106.0<sup>a</sup></b>	105.6	106.2	106.2	106.3	106.0	106.0	106.3
O <sub>1</sub> -C <sub>2</sub> -H <sub>6</sub>	<b>115.9<sup>a</sup></b>	116.2	115.7	115.7	115.4	115.8	115.9	115.4
C <sub>3</sub> -C <sub>2</sub> -H <sub>6</sub>	<b>133.4<sup>a</sup></b>	132.9	133.8	133.9	134.1	133.7	133.8	134.1
C <sub>2</sub> -C <sub>3</sub> -H <sub>7</sub>	<b>126.1<sup>a</sup></b>	126.8	126.2	126.2	126.6	126.5	126.5	126.6
C <sub>4</sub> -C <sub>3</sub> -H <sub>7</sub>	<b>127.9<sup>a</sup></b>	127.6	127.6	127.5	127.1	127.5	127.4	127.1
Dipole moment	<b>0.66<sup>a</sup></b>	0.77	0.64	0.87	0.60	0.63	0.52	0.64

<sup>a</sup>Reference [54]

**Notes: DFT B3LYP as highlighted in the table captures very well both the bond length and the dipole moment in comparison to experimental values.**

**Table 2.4: Polarizability components for furan calculated as different levels of theory and basis sets**

Method	$\langle\alpha\rangle$	$\Delta\alpha$
This work (B3LYP/ 6-31+ (3d,3p	48.72	21.098
B3LYP/pol	49.71 <sup>a</sup>	22.69 <sup>a</sup>
B3LYP/(+sd+sp)	47.57 <sup>a</sup>	22.25 <sup>a</sup>
MP2/ 6-31+G(d,p)	43.6 <sup>b</sup>	19.1 <sup>b</sup>
MP2/ C	48.5 <sup>c</sup>	20.6 <sup>c</sup>
<b>Exp</b>	<b>49.12<sup>d</sup></b>	<b>21.98<sup>d</sup></b>
% deviation, this work to experimental values	0.81	4.01

<sup>a</sup>reference[52], <sup>b</sup>reference[55], <sup>c</sup>reference[62], <sup>d</sup>reference[63]

**Notes: Percentage deviations of our theoretical calculations of polarizability components as compared to experimental findings show that they is high correlation between calculated and experimental values.**

**Table 2.5: Experimental and Theoretical dipole moment ( $\mu$ ) of furan calculated using different model chemistries**

method	$\mu$ (DEBYE)
B3LYP/ 6-31+G(3d,3p)	0.66
B3lyp /pol	0.83 <sup>a</sup>
HF/ pol	1.03
SCF/ 6-31G*	0.86 <sup>b</sup>
SCF/B	0.79
SCF/C	0.82
MP2/B	0.62
MP2/C	0.65
MP2/ 6-31G*	0.68
EXP	0.661 0.006 <sup>c</sup>

<sup>a</sup>reference[52], <sup>b</sup>reference[63], <sup>c</sup>reference[54]

### 3 RESULTS AND DISCUSSION

#### 3.1 Equilibrium structures

The geometries of DFM molecular structures were optimized without considering symmetry constraints, using Gaussian '09 package with B3LYP/6-31+G(3d,3p) method. The nature of stationary point was evaluated using harmonic frequency analysis and it was confirmed to be a local minimum in the potential energy surface. The potential energy surface scanning tool (PESST) [64] was used to generate 12 conformational structures of DFM, by varying the angle between two furanic rings at an increment of 30 degrees. The geometric parameters of DFM such as equilibrium bond lengths ( $r_e$ ) and bond angles ( $\Theta_e$ ) were calculated using DFT (B3LYP) theoretical method and 6-31+G(3d, 3p) basis set as listed in Table 3.1 and 3.2 the equilibrium structure is depicted in Figure 3.1

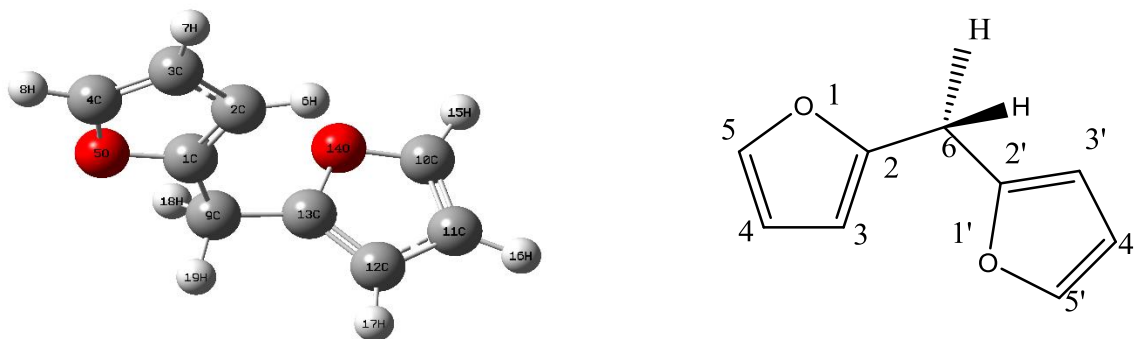


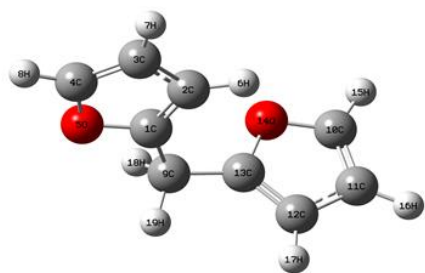
**Figure 3.1: Equilibrium structure of DFM (Global minimum) and the Equilibrium structure of DFM (showing numbering according to IUPAC)**

**Table 3.1: Equilibrium bond distance ( $r_e$ ) of DFM calculated at B3LYP/6-31+G (3d, 3p) in Angstroms**

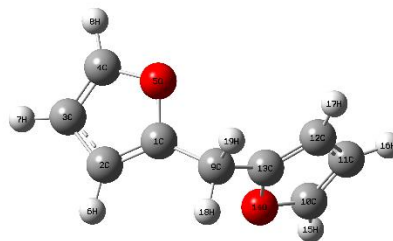
Bond type	$r_e$
$r(\text{C}_1=\text{C}_2) = r(\text{C}_{12}-\text{H}_{13})$	1.363
$r(\text{C}_1-\text{O}_5) = r(\text{C}_{13}-\text{H}_{14})$	1.369
$r(\text{C}_1-\text{C}_9) = r(\text{C}_9-\text{C}_{13})$	1.496
$r(\text{C}_2-\text{C}_3) = r(\text{C}_{11}-\text{C}_{12})$	1.436
$r(\text{C}_2-\text{H}_6) = r(\text{C}_{12}-\text{H}_{17})$	1.080
$r(\text{C}_3=\text{C}_4) = r(\text{C}_{10}=\text{C}_{11})$	1.359
$r(\text{C}_3-\text{H}_7) = r(\text{C}_{11}-\text{H}_{16})$	1.080
$r(\text{C}_4-\text{O}_5) = r(\text{C}_{10}-\text{O}_{14})$	1.366
$r(\text{C}_4-\text{H}_8) = r(\text{C}_{10}-\text{H}_{15})$	1.078
$r(\text{C}_9-\text{H}_{18}) = r(\text{C}_9-\text{H}_{19})$	1.095

**Table 3.2: Equilibrium bond angles ( $\theta_e$ ) of DFM calculated at B3LYP/631+G(3d,3p) in degrees**

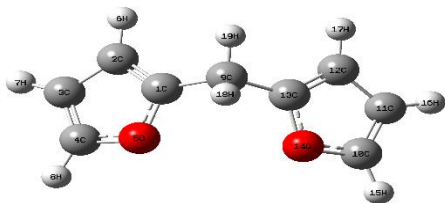
Bond angle type	$\theta_e$
$\theta$ (C <sub>2</sub> =C <sub>1</sub> -O <sub>5</sub> )	09.7
$\theta$ (C <sub>2</sub> =C <sub>1</sub> -C <sub>9</sub> )	133.4
$\theta$ (O <sub>5</sub> -C <sub>1</sub> -C <sub>9</sub> )	116.9
$\theta$ (C <sub>1</sub> =C <sub>2</sub> -C <sub>3</sub> )	106.6
$\theta$ (C <sub>1</sub> =C <sub>2</sub> -C <sub>6</sub> )	126.0
$\theta$ (C <sub>3</sub> -C <sub>2</sub> -H <sub>6</sub> )	127.4
$\theta$ (C <sub>2</sub> -C <sub>3</sub> =C)	106.1
$\theta$ (C <sub>2</sub> -C <sub>3</sub> -H <sub>7</sub> )	127.5
$\theta$ (C <sub>4</sub> =C <sub>3</sub> -H <sub>7</sub> )	126.4
$\theta$ (C <sub>3</sub> =C <sub>4</sub> -O <sub>5</sub> )	110.3
$\theta$ (C <sub>3</sub> =C <sub>4</sub> -H <sub>8</sub> )	133.8
$\theta$ (O <sub>5</sub> -C <sub>4</sub> -H <sub>8</sub> )	115.9
$\theta$ (C <sub>1</sub> -O <sub>5</sub> -C <sub>4</sub> )	107.3
$\theta$ (C <sub>1</sub> -C <sub>9</sub> -C <sub>13</sub> )	114.7
$\theta$ (C <sub>1</sub> -C <sub>9</sub> -H <sub>18</sub> )	107.7
$\theta$ (C <sub>1</sub> -C <sub>9</sub> -H <sub>19</sub> )	107.7
$\theta$ (C <sub>13</sub> -C <sub>9</sub> -H <sub>18</sub> )	109.7
$\theta$ (C <sub>13</sub> -C <sub>9</sub> -H <sub>19</sub> )	107.7
$\theta$ (H <sub>18</sub> -C <sub>9</sub> -H <sub>19</sub> )	107.1
$\theta$ (C <sub>11</sub> =C <sub>10</sub> -O <sub>14</sub> )	110.3
$\theta$ (C <sub>11</sub> -C <sub>10</sub> -H <sub>15</sub> )	133.8
$\theta$ (O <sub>14</sub> -C <sub>10</sub> -H <sub>15</sub> )	115.9
$\theta$ (C <sub>10</sub> -C <sub>11</sub> -H <sub>12</sub> )	106.1
$\theta$ (C <sub>10</sub> -C <sub>11</sub> -H <sub>16</sub> )	126.4
$\theta$ (C <sub>12</sub> =C <sub>11</sub> -H <sub>16</sub> )	127.5
$\theta$ (C <sub>11</sub> -C <sub>12</sub> -H <sub>17</sub> )	127.4
$\theta$ (C <sub>13</sub> =C <sub>12</sub> -H <sub>17</sub> )	126.0
$\theta$ (C <sub>9</sub> -C <sub>13</sub> =C <sub>12</sub> )	133.4
$\theta$ (C <sub>9</sub> -C <sub>13</sub> -O <sub>14</sub> )	116.8
$\theta$ (C <sub>12</sub> -C <sub>13</sub> =O <sub>14</sub> )	109.7
$\theta$ (C <sub>11</sub> -C <sub>12</sub> -H <sub>17</sub> )	127.4
$\theta$ (C <sub>13</sub> =C <sub>12</sub> -H <sub>17</sub> )	126.0
$\theta$ (C <sub>9</sub> -C <sub>13</sub> =C <sub>12</sub> )	133.4



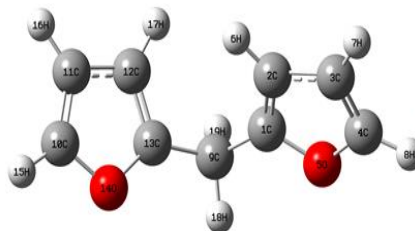
*Conformer 1*



*Conformer 2, global minimum*



*Conformer 3*



*Conformer 4*

**Figure 3.2: Conformational structures of DFM molecule**

The energetics and pictorial representations of 4 equilibrium conformational structures of DFM are depicted in Table 3.3 and Figure 3.2.

**Table 3.3: Different energetics of 4 conformers of DFM molecule**

Conformer	Energy (kcal/mol)
1	0.0903
2	0.000
3	0.0156
4	0.254

## 3.2 Infrared spectral data

The IR spectrum for DFM obtained from DFT, B3LYP/6-31+G(3d,3p), shows fifty one (51) fundamental bands (modes). This is in accordance with the  $3N-6$  rule for non-linear molecules which in this case suggests the absence of Fermi resonance effect (degenerate fundamental bands) or infrared inactive symmetric stretch or crowding of peaks and low intensities that can result in poor resolution. It can be deduced that the model chemistry employed in the harmonic frequency calculation can accurately describe quadratic part of the potential energy surface (PES) due to the inclusion of correlation and relatively large basis set [65]–[68].

There is a good correlation between calculated (B3LYP/6-31+G(3d,3p)) and experimentally (FTIR) obtained IR spectral data. The harmonic frequency method was employed for the description of force fields without scaling of the results against experimental values to avoid losing physical meaning of the PES (the use of scale factor bears no information about the harmonicity and anharmonicity of the PES) [65].

The experimental FTIR and computational DFT-IR spectra are compared using vibrational modes and intensities of several peaks. The two IR spectra match as depicted in Figures 3.2.a and 3.2.b.



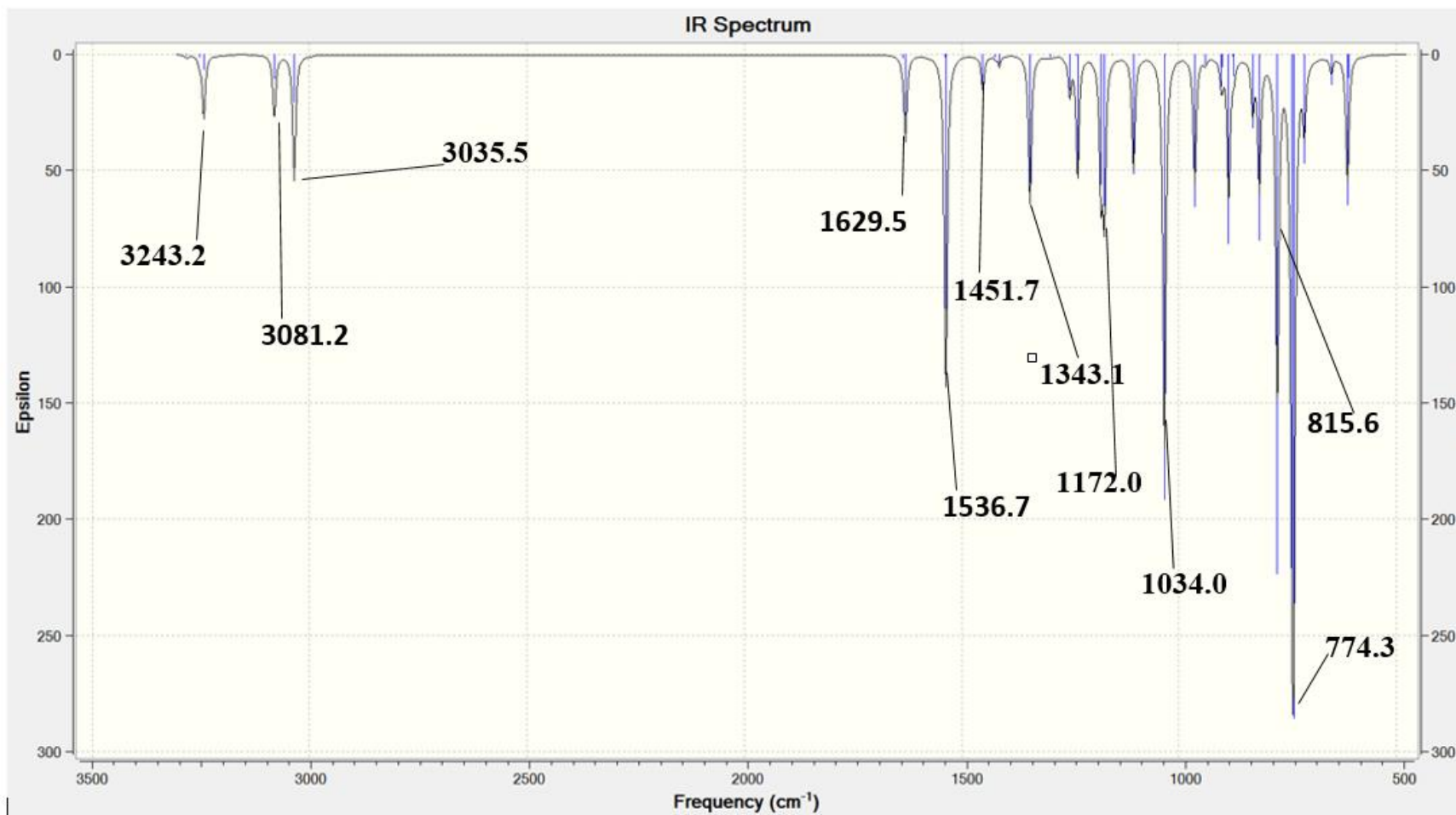
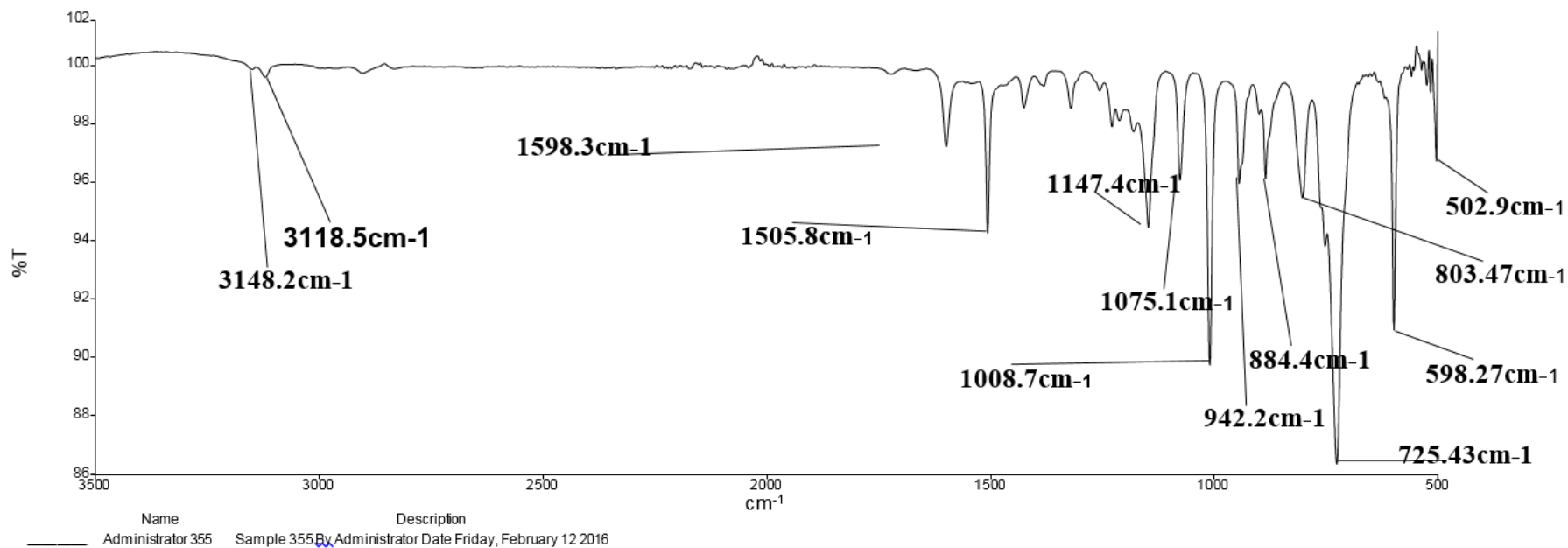
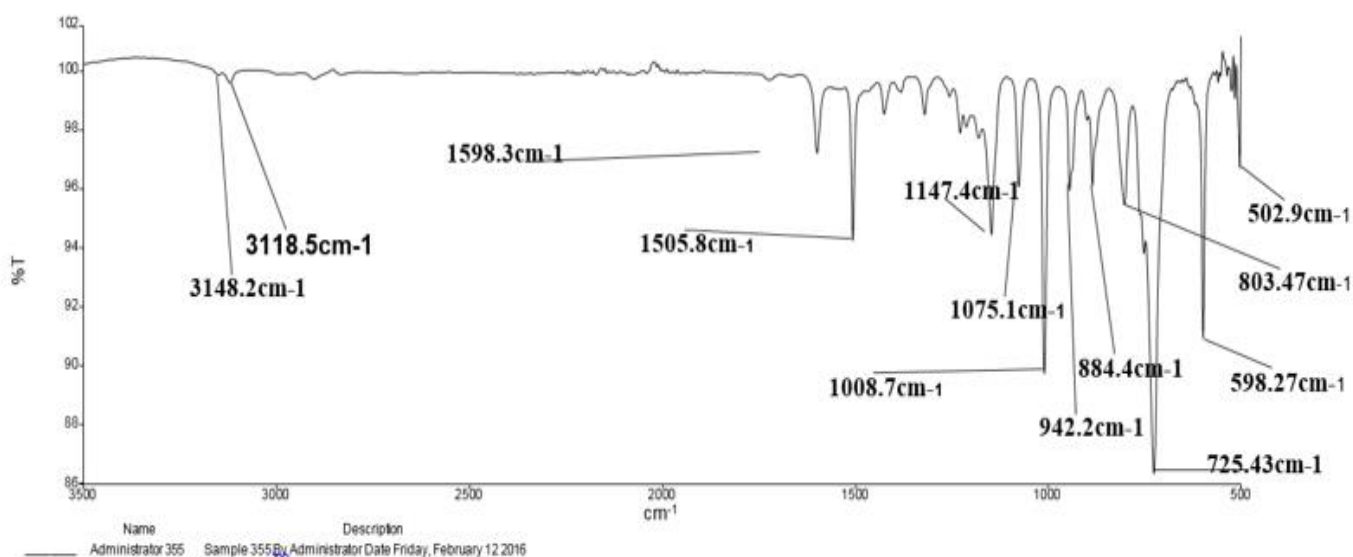
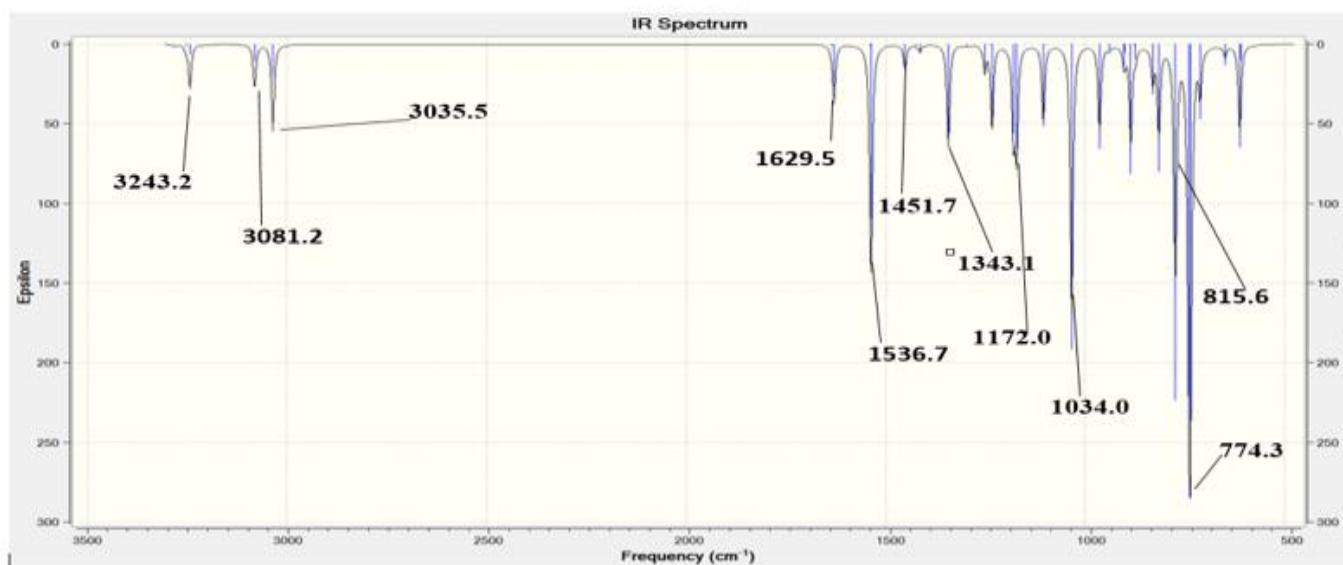


Figure 3.2 a: Calculated IR spectrum of DFM calculated at B3LYP/ +G (3p, 3p) DFM molecule



**Figure 3.2 b: Experimental IR spectrum of DFM molecule**



**Figure 3.2 c: Experimental and calculated IR spectra for DFM molecule**

The calculated DFT harmonic vibrational frequencies are reported in Table 3.4. They are compared with the experimental FTIR spectral analysis. We observe small discrepancy between experimental FTIR data and DFT-IR calculations in part due to non-scaling, anharmonicity and basis set incompleteness error (BSIE).

**Table 3.4: Experiment and calculated Harmonic frequencies and intensities calculated at B3LYP +G 631(3d, 3p), DFM molecule**

Vibrational mode	$\nu_{\text{Theo}}$ ( $\text{cm}^{-1}$ )	$\nu_{\text{exp}}$	$I_{\text{Theo}}$	$\% \Delta \nu$
=CH (Olefin asymmetric stretch)	3243.2	.....	.....	.....
-CH <sub>2</sub> (aliphatic asymmetric stretch)	3081.2	3148.2	8.1	-2.2
-CH <sub>2</sub> (aliphatic symmetric stretch)	3035.5	3118.5	15.7	-2.7
C=C (Furanic residue)	1629.5	1598.3	10.6	-1.9
C=C (Furanic ring)	1536.7	1505.8	42.2	-2.0
CH <sub>2</sub> (Scissoring)	1451.7	1424.4	4.6	-1.9
CH <sub>2</sub> (See saw)	1343.1	1320.2	18.6	-1.7
COC (Furanic residue)	1251.8	1211.4	4.8	-3.3
COC (Furanic ring)	1172.0	1147.4	19.1	-.2.1
=CH (Breathing mode)	1034.0	1008.7	49.6	-2.4
Out of plane	815.6	803.5	16.4	-1.5
Out of plane	774.3	725.4	43.4	-6.3
Out of plane	736.5	598.3	52.7	-18.7

The analysis of corresponding peaks between the overlapping IR spectra in Figure 3.2.c is outlined as follows:

**C-H vibrational mode:** The hetero-aromatic structure shows the presence of calculated CH stretching band at  $3243.21\text{ cm}^{-1}$  and the FTIR peak at  $3117.8\text{ cm}^{-1}$ .

**Out-of-plane C-H bending modes:** According to Kalsi and co-workers [69]: substitution patterns on the ring can be judged from the out-of-plane bending of the ring C-H bands in the region  $900 - 675\text{ cm}^{-1}$  for furan. The calculated band of out-of-plane bending deformations for DFM is identified at  $815.6, 774.3$  and  $736.5\text{ cm}^{-1}$  these agrees well with FTIR (peaks) results that resonate at  $803.5$  and  $725.4\text{ cm}^{-1}$  with an average percentage difference of  $-1.55\%$ . The DFM molecule can be easily described by substitution patterns on its furanic ring as they are three C-H bands from IR spectra but only two C-H bands would be observed in the case of mono-furanic ring structure; because furan is a highly symmetric molecule with a  $C_{2v}$  point group. Therefore only two out-of-plane C-H bending modes are anticipated, for DFM this symmetry pattern is broken due to the presence of  $\text{CH}_2$  substituent bridge between two furanic rings.

**Ring vibration:** In DFM, the ring vibrations appear to be mixed among the modes shown in Table 3.3. The position and intensity of these vibrations are dependent on the nature of the ring and the type of substitution [70]. Billes and co-workers reported a vibrational spectroscopic study on furan and its hydrated derivatives [71] and they closely resemble the IR spectral data of DFM molecule.

**C=C vibrational mode:** The DFM calculated modes are in the regions  $1629.5$  and  $1536.7\text{ cm}^{-1}$  in good agreement with FTIR vibrational modes at  $1598.3$  and  $1505.8\text{ cm}^{-1}$ .

**COC vibrational mode:** The FTIR band for COC aromatic stretch can be identified at  $1147.4$  and is theoretically calculated to be  $1172.0\text{ cm}^{-1}$ .

The average percentage ( $\sim 5.0\%$ ) discrepancy for stretching frequency is higher than those of bending (at  $\sim 2\%$ ) due to the more pronounced effect of anharmonicity within the stretching mode as more forces are applied to the bonds thus forcing them to depart from a harmonic description

[65].

**Note: Some peaks were not labelled during data compilation and are represented by gaps as they do not adversely affect the comparison of the two overlapping spectra.**

### **3.3 Gauge Independent Atomic Orbital (GIAO) calculated chemical shifts and 1-dimensional experimental proton nuclear magnetic resonance (1-Dimensional $^1\text{H-NMR}$ ) chemical shifts**

NMR chemical shifts and coupling constants are mixed second derivative properties of electronic energy against magnetic field and magnetic dipole moment. The introduction of a magnetic field in the electronic Schrödinger equation results in the occurrence of the “gauge problem.” Whereby our calculations inherently depend on the origin of the coordinate system; magnetic field does not directly depend on the gauge. Since magnetic field is a function of a vector potential that depends on the gauge therefore the magnetic field is somehow linked to the gauge origin in that manner. One of the best remedy to the gauge problem is to develop methods of calculation that are gauge independent [72], and to date the most robust conventional gauge independent method is the gauge independent atomic orbital (GIAO) developed by London in 1937 [72].

The GIAO calculations are known to be very proficient in determining NMR shielding tensors [73]. In computation of isotropic chemical shielding tensors, Gauge Independent Atomic Orbital (GIAO) calculation method was employed with iglo-2 basis sets. The GIAO calculations were done on optimized geometries of DFM. The calculated chemical shift ( $\delta_{\text{calc}}$ ) is determined as shown below:

$$\delta_{\text{calc}} = \sigma_{\text{tms}} - \sigma_{\text{iso}} \quad (3)$$

Where  $\sigma_{\text{tms}}$  and  $\sigma_{\text{iso}}$  are isotropic shielding tensors for a reference molecule (Tetramethyl silane) and difurylmethane (DFM) respectively.

Previous work from literature was reported using correlation between experimental ( $\delta_{\text{exp}}$ ) and calculated ( $\delta_{\text{calc}}$ ) chemical shifts [73], [74], in the following equation:

$$\delta_{\text{exp}} = a \times \delta_{\text{calc}} + b \quad (4)$$

Where a and b give slope (a) or (first derivative of  $\delta_{\text{exp}}$  with respect to

$\delta_{\text{calc}}$ ) and it is the intercept between the experimental and the calculated shifts; these terms (a and b) bears no physical importance but they arise due to the subsequent plot of  $\delta_{\text{exp}}$  against  $\delta_{\text{calc}}$  and they are linked to the valuation of the theoretical chemical shifts to the experiment. The idealized situation is when the values of a and b are 1 and 0, respectively and in that case; the theoretical data precisely matches the experiment. In our work, we are using GIAO calculations where the gauge origin is localized in the center of the field dependent orbitals (GIAO is a method that uses functions that have inherent dependence on external magnetic field), the gauge origin is localized to the center of basis functions and matrix elements rearranged to be independent of the origin.

In NMR, electrons generate secondary magnetic fields described by paramagnetic and diamagnetic terms. When the secondary field is aligned with the external field, paramagnetic term takes root but when it is anti-parallel to the field it describes a diamagnetic term. During the early years of quantum NMR shielding calculations, the origin of the field was taken to be localized in the nucleus but this were found to drift drastically when doing calculations because in a given molecule there are several nuclei. This subsequently results in obtaining different terms for secondary magnetic fields (paramagnetic and diamagnetic term mismatch). This anomaly is offset by fixing the gauge origin within the field dependent atomic centers rather than in the nucleus. We can offset this discrepancy by eliminating the paramagnetic term [73].

The use of density functional theory (DFT) with more advanced basis sets gives more precise results. Rablen et al [75] showed that the use of hybrid functionals like B3LYP give very accurate results for many organic compounds. Bagno and co-workers also showed that using B3LYP and moderately large basis set gives reasonably precise magnetic parameters [76].

In the literature  $^1\text{H}$ -NMR GIAO calculations are not numerous due to the fact that proton chemical shifts are very small and often overlap with the region associated with the solvent effect [72].

Errors in NMR calculations might arise from sources, such as electron correlation and rotational-

vibrational effects and incompleteness of the basis set. Many errors in the calculated chemical shift from single point of the reference compound will be reflected in all derived chemical shift. Subtracting the chemical shift of the reference can also compensate for general discrepancy in magnitude of the predicted absolute shielding. Borkowski and coworkers [73] hold the hypothesis that, it is also reasonable to consider parameters derived from shielding tensor to take into account the anisotropy which cannot be eliminated by orientational averaging of conformation energy or chemical shifts. Some of the errors can be offset by calculating weighted average of chemical shifts and by scaling shielding tensors to experimental chemical shifts.

The correlation between experimental and calculated chemical shifts is shown in Figure 3.3 and the values are listed in Tables 3.5, 3.6 and 3.7. The plot shows correlation coefficient (0.9842) with some discrepancy in peak at  $\delta = 6.362$ , 4, (7, 16) and  $\delta = 6.143$ , 3, (6, 17): The numbers in brackets refer to numbering in the Gaussian model. The order of chemical shifts between these peaks is inconsistent with experimental shifts. Hypothetically it is expected that protons (7, 16) to resonate at a frequency/chemical shift higher than that associated with protons (6, 17), mainly because the proposed configuration agrees well with the clockwise electron flow in the furan ring. This clockwise flow of electrons in resonance structure of furan as opposed to the anticlockwise direction of resonance places a negative charge at carbon 3 (proton 6, 17) and 5 (8, 15) (carbons numbered according to IUPAC). Thus in comparison to proton (7,16) proton (6,17) is more shielded by virtue of lone pair of electrons situated at carbon 3. Thus due to the influence of inductive effect the peaks should follow the ordering given by experimental NMR data.

There are four terms which are relevant to  $J_{\max}$  or coupling constant, diamagnetic and paramagnetic, spin orbit terms, spin dipole and Fermi contact term.  $J_{\max}$  is sensitive to the type of functional and basis set chosen. The Gaussian type orbitals (GTOs) like 6-31+G (3d,3p) do not produce the correct cusp of the nuclei. Koch and Holthausen [77] recommend the use of IGLO-II and -III basis sets for proton NMR. The theoretical coupling constants are depicted in table 3.6.

The experimental  $^1\text{H-NMR}$  (Figure 3.4) of DFM molecule shows a singlet (s) at  $\delta_{\text{H-6}} = 4.057$  due to the  $-\text{CH}_2-$  protons, the molecule is taken to be symmetrical therefore similar protons are represented by one proton position. The spectrum also shows a doublet of doublet at  $\delta_{\text{H-5}} = 7.391$



(2H, dd,  $J_{3,5} = 0.733$  and  $J_{4,5} = 1.953$  Hz), whereby J represents coupling constants for proton 8. Furthermore another doublet of doublet is shown at  $\delta_{H-4} = 6.362$  (2H, dd,  $J_{4,5} = 1.953$  and  $J_{3,4} = 3.175$  Hz) for proton 4. A doublet of doublet is shown at  $\delta_{H-3} = 6.1425$  (2H, dd,  $J_{3,5} = 0.733$  and  $J_{3,4} = 3.175$  Hz) corresponding to proton 3.

This data is depicted in Table 3.6 and it is quite clear that proton 5 have at least one common coupling constant which can be associated with protons 3 and 4 therefore it couples with both of them. Similarly these applies to protons 4 being split by protons 4 and 5. Even proton 3 couples with 4 and 5 by virtue of common coupling constants.

All this information obtained from experimental 1-Dimensional  $^1\text{H-NMR}$  (300 MHz) clearly helps us to characterize molecular structure of DFM.

Correlation diagram of experimental against calculated chemical shift (ppm)

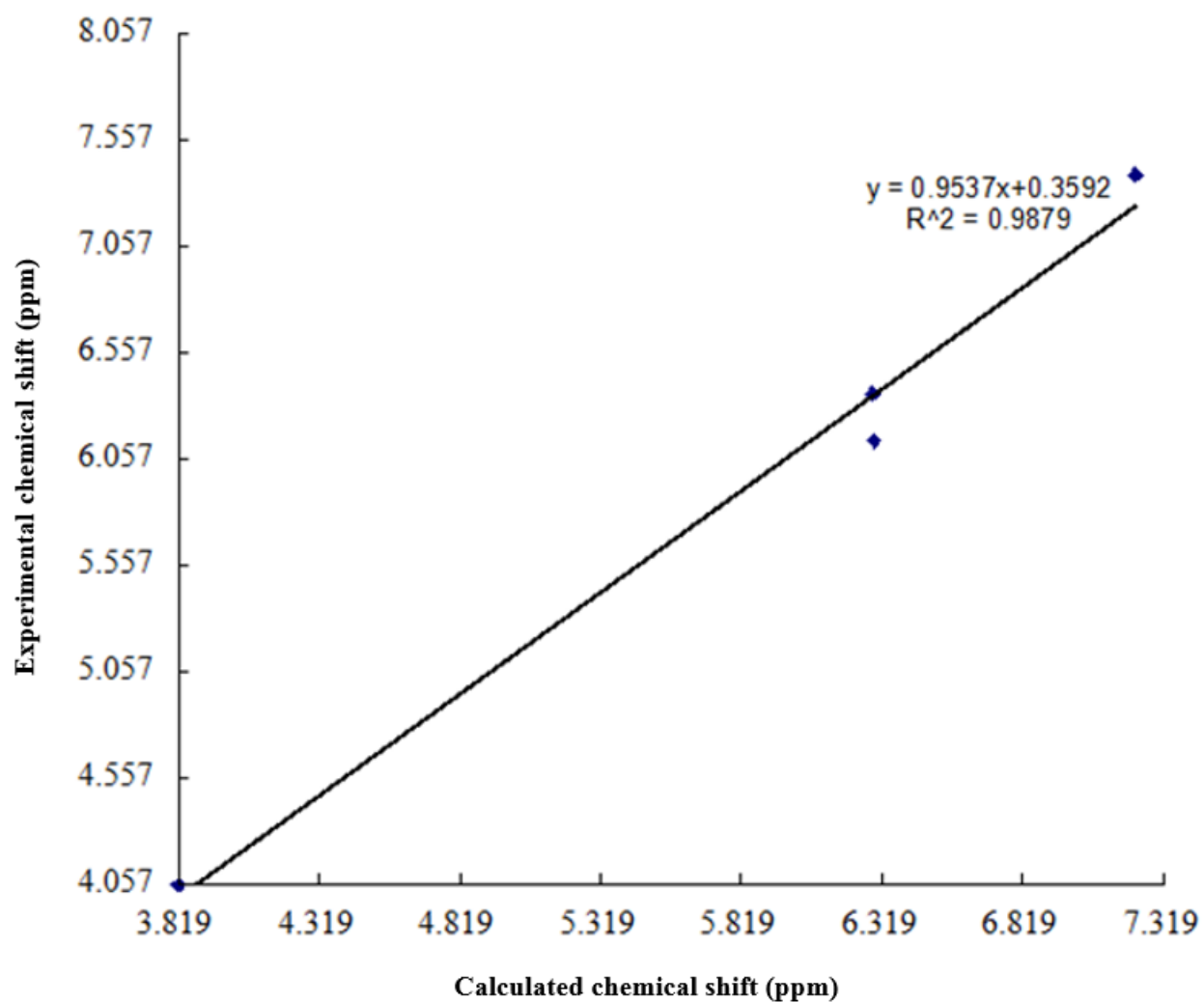


Figure 3.3: Experimental and calculated proton NMR spectra for DFM molecule calculated at B3LYP/ 6-31+G(3d, 3p)

**Table 3.5: NMR chemical shifts obtained from experimental and calculated at B3LYP/IGLO-2 for DFM MOLECULE. TMS,  $\sigma_{\text{iso}}=32.0092$  (IUPAC numbering system is represented as H-3, H-4, H-5 and H-6 and are highlighted)**

Position	$\sigma_{\text{iso}}$	$\delta_{\text{cal}}$	$\delta_{\text{exp}}$
8, 15 ( <b>H-5</b> )	24.788, 24.787	7.218	7.391
7, 16 ( <b>H-4</b> )	25.726, 25.726	6.284	6.362
6, 17 ( <b>H-3</b> )	25.717, 25.723	6.289	6.143
18, 19 ( <b>H-6</b> )	28.191, 28.190	3.819	4.057

**Table 3.6: Theoretical NMR nuclear coupling constants**

Peak assignments	8	7	6
8, 15 ( <b>H-5</b> )	-	-1.18919 Hz	-2.18809 Hz
7, 16 ( <b>H-4</b> )	-	-	-0.929184 Hz

**Table 3.7:  $^1\text{H}$ -NMR (300 MHz NMR data for difurylmethane in  $\text{CDCl}_3$ )**

position	$\delta_{\text{H}}$ (ppm)
8, 15 ( <b>H-5</b> )	7.391 (2H, dd, $J_{3,5}=0.733$ and $J_{4,5}=1.953$ Hz)
7, 16 ( <b>H-4</b> )	6.362 (2H, dd, $J_{4,5}=1.953$ and $J_{3,4}=3.175$ Hz)
6, 17 ( <b>H-3</b> )	6.143 (2H, dd, $J_{3,5}=0.733$ and $J_{3,4}=3.175$ Hz)
18, 19 ( <b>H-6</b> )	4.057 (2H, s)

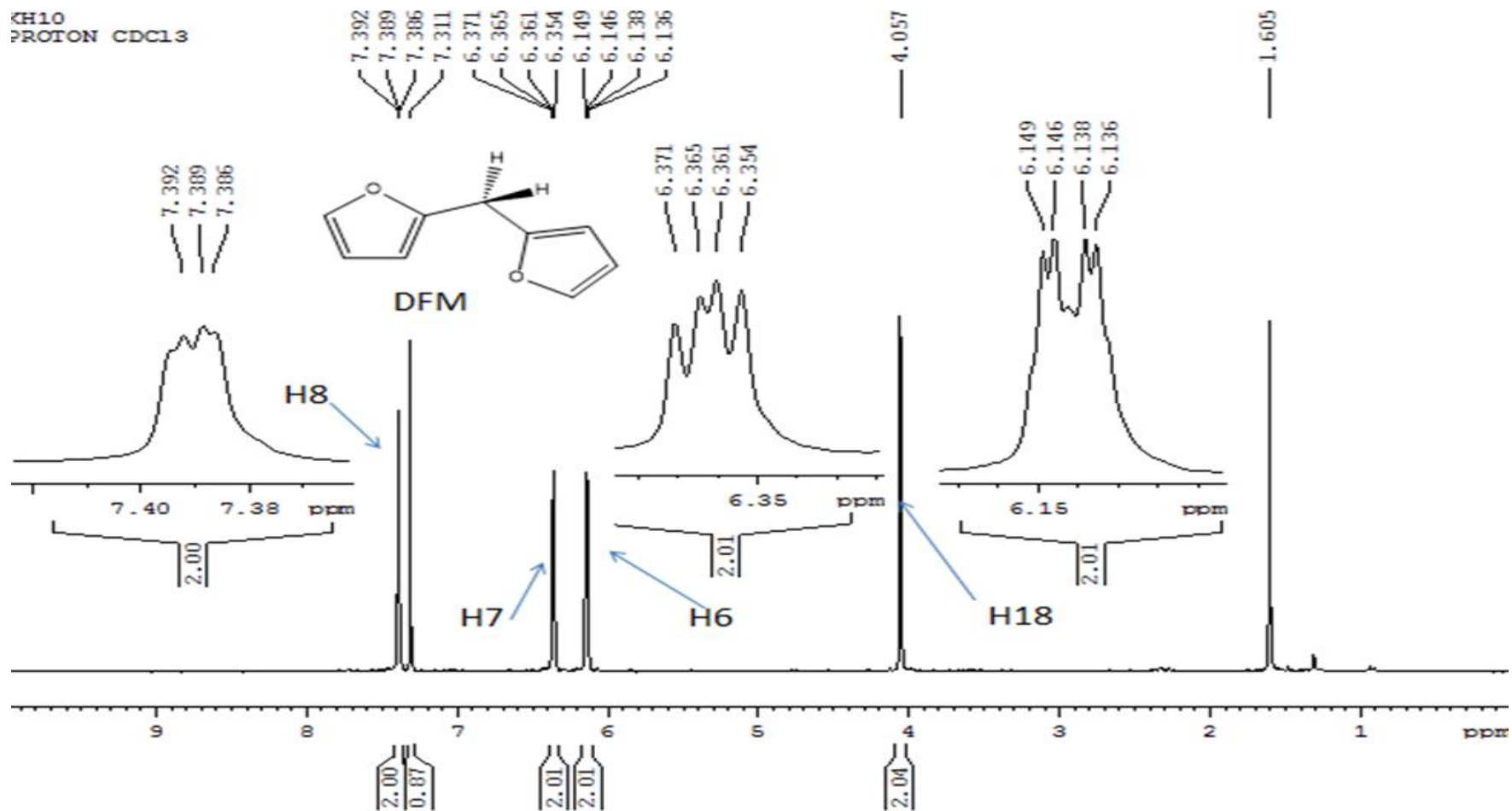


Figure 3.4: Experimental  $^1\text{H}$ - NMR spectrum of DFM in  $\text{CDCl}_3$

### 3.4 Geometric Parameters of DFM-Methanol adducts

The Oxygen atom in DFM with lone pairs and the polarized  $\pi$ -system of the furanic ring offer two probable sites that serve as hydrogen bond acceptors to the proton in the hydroxyl (O-H) group of methanol. Two types of configurations classified as  $\sigma$ -type and  $\pi$ -type hydrogen bonding have been indicated as depicted in Figure 3.5 and 3.6 following geometric optimization at B3LYP/6-31+G(3d,3p) level of theory. The  $\sigma$ -type configuration is the binding scheme whereby the acidic proton of -OH group in MeOH is facing the DFM oxygen atom and  $\pi$ -type configuration is the scheme where the acid proton is pointing towards the  $\beta$ -carbon in the furanic ring of DFM.

The basis set superposition error (BSSE) and thermal energy (calculated under the harmonic-rigid rotor approximation) corrected stabilization energies associated with the  $\sigma$ -type and  $\pi$ -type configurations are -3.16 and -1.89 kcal/mol, respectively as depicted in Table 3.9. These values are compared to -1.79 ( $\sigma$ -type) and -1.08 ( $\pi$ -type) kcal/mol literature data obtained for furan-MeOH complex computed by Xiatong and co-workers [78] working at B3LYP/ Aug-cc-PVTZ level of theory. The enthalpies of formation and Gibbs free energy for  $\sigma$ -type complex were calculated as -1.97 and 5.64 kcal/mol, respectively. It is quite evident from the negative value of enthalpy of formation, that complexation of Methanol and DFM is quite favourable at low temperatures and due to the small value of equilibrium constant (positive value of  $\Delta G$ ) the reaction is less feasible in the forward direction. The enthalpy of formation and Gibbs free energy for  $\pi$ -type dimer is -0.75 and 5.66 kcal/mol, respectively.

From the rigid scan results, we conclude that the interaction of the proton of the hydroxyl group of MeOH with charge density around the hetero atom of DFM in Figure 3.5 is the most favorable  $\sigma$ -type of hydrogen bonding, as it is the interactive scheme with the minimal energy. Furthermore, a redundant potential energy scan was performed on the  $\pi$ -type hydrogen bonding configuration and it was established that the bonding scheme whereby the acidic proton of MeOH interacts with the  $\beta$ -carbon in the furanic ring is most stable among the  $\pi$ -type configurations. But between the two local minima ( $\sigma$ -type and the  $\pi$ -type configurations); the  $\sigma$ -type hydrogen bonding configuration is the most stable because it has larger stabilization energy ( $\Delta E = 1.27$  kcal/mol) between the two configurations. Similar results were obtained in the study of furan-HCl complex [31]. In a different study Kgagodi and Mbaiwa did similar study on DFM-n-propanol binary

mixture (employing Molecular Mechanics and ab-initio methods) looking at the thermodynamic properties and structure. The data obtained from radial distribution functions and ab-initio calculations show evidence of hydrogen bonding between n-propanol and DFM via the acidic hydrogen MeOH and the hetero atom of DFM [79]. The results they obtained from radial distribution functions showed a broad, low intensity peak centred at 2.21 Å corresponding to the distance between the hetero atom of furan and acidic proton of hydroxyl group of propanol and this distance was calculated to be 2.20 using *ab initio* methods with HF/6-31 G(d) model chemistry. The results obtained in these study for  $\sigma$ -type complex was calculated to be 2.09 Å, which is slightly lower than those obtained for DFM-Propanol dimer. The reason for this difference might be due to the accuracy of different model chemistries employed in each case and also due to the fact that two different types of complexes are being compared. Hartree-Fock in general using constrained methods tends to underestimate bond lengths. This is mainly due to the exclusion of electron correlation compared to unrestricted Hartree-Fock, Density functional theory and correlation methods. In the computational calculations employed in these work B3LYP/6-31 +G (3d,3p) method was employed.

In the current study, it is evident that the extent of O-H bond elongation found among the two local minima complexes is more profound within the  $\sigma$ -type configuration in comparison to the  $\pi$ -type. This can be used to emphasize that hydrogen bonding is more pronounced within the  $\sigma$ -type binding configuration. The change associated with the O-H bond length (bond elongation) during hydrogen bonding closely resembles those observed in classical hydrogen bonding, where the O-H bond length elongates [24], [54]. This is the common feature observed in both configurations present in the DFM-MeOH complexes. The change in O-H bond length for  $\sigma$ -type hydrogen bonded DFM-MeOH complex was calculated to be 0.97 Å, a closely similar value (0.96 Å) was computed by Xiatong and co-workers [78] on furan-MeOH complex. The O-H elongation value for  $\pi$ -type DFM-MeOH complex in this work was calculated at 0.97 Å, whilst the value obtained in the literature by Xiatong and co-workers is 0.96Å for furan-MeOH. Consequently there is smaller bond elongation for  $\pi$ -type system compared to the  $\sigma$ -type system. The O-H bond elongation in both complex is due to the effective pulling of the acidic proton of the hydroxyl group of MeOH by the either of the two lewis bases ( heteroatom and the  $\beta$ -carbon of the polarized  $\pi$ -system) thus weakening the O-H bond and causing it to elongate. This effect is more pronounced

in the  $\sigma$ -type configuration because oxygen is a stronger lewis base than the polarised  $\pi$ -system.

The IR spectral data on DFM-MeOH complex clearly shows red shifts in the OH vibrational transitions on both adducts configurations which is consistent with presence of hydrogen bonding in hetero-aromatic systems, This is consistent with what have been obtained by Xiatong and co-workers on IR spectral transitions of furan-MeOH [78], [80]–[83]. The IR spectroscopy data and geometries of DFM-MeOH complex is depicted in Table 3.8. The red shift frequency for  $\sigma$ -type configuration from O-H fundamental band ( $3820.70\text{ cm}^{-1}$ ) in methanol was found to be  $66.83\text{ cm}^{-1}$  and that in a  $\pi$ -type configuration was calculated at  $74.18\text{ cm}^{-1}$ . This is somewhat inconsistent with previous [78] experimental findings that indicate that  $\sigma$ -type dimer is more red shifted due to its stronger classical nature of hydrogen bonding compared to  $\pi$ -type dimer that undergoes non-classical less stronger hydrogen bonding. The red shift is used to index the strength of O-H bond or force constant. The  $\sigma$ -type complex is associated with larger elongation of O-H bond length and thus larger red shift. This is not observed in our computational results due to the nature of B3LYP to overestimate the O-H stretch of O-H...O configuration.

The  $\sigma$  and  $\pi$ -type complexes have higher intensities (262.0429, 259.3501 kJ/mol) for O-H bond, compared to the intensity of O-H stretching band in the reference (32.7250 kJ/mol) molecule (MeOH) indicative of significance of high oscillation of transition moment, a required characteristic for IR absorption and also a requirement associated with the red shift. The  $\sigma$ -type dimer have higher intensity (262.0429 kJ/mol) for OH bond than  $\pi$ -type dimer (259.3501 kJ/mol) due to large polarisation of OH bond length by the heteroatom.. This is a prerequisite for IR absorption or peak intensity.

**Table 3.8: The calculated O-H bond in the DFM-MeOH complex and intermolecular bond distance and bond angles.**

Complex	R (O-H) <sup>a</sup>	$\Delta R$ (O-H) <sup>b</sup>	$\Theta$ <sup>c</sup>	$\nu$ <sup>e</sup>	$\Delta\nu$ <sup>f</sup>	$I$ <sup>g</sup>
$\pi$ -type R (O-H)	0.96597	0.00326	164.169	3746.52	74.18	259.3501
$\sigma$ -type R (O-H)	0.96647	0.00376	162.658	3753.87	66.83	262.0429
Free R (O-H)	0.96271 <sup>d</sup>	.....	.....	3820.70	.....	32.7250
$\sigma$ -type R (O-H...O))	2.09103	.....	.....	.....	.....	.....

<sup>a</sup>OH bond length in the complex in angstroms, <sup>b</sup>change of bond length upon complexation in angstroms, <sup>c</sup>intermolecular hydrogen bond angle, <sup>d</sup>OH bond length in unbounded methanol, <sup>e</sup>vibrational frequency ( $\text{cm}^{-1}$ ), <sup>f</sup>shift in vibrational frequency ( $\text{cm}^{-1}$ ), <sup>g</sup>IR intensities (kJ/mol)

**Table 3.9: Calculated binding energy (BE<sup>a</sup>), Counterpoise energy ( $\Delta E^{\text{CP}}$ )<sup>b</sup>, Energy for Methanol (E<sup>c</sup>) and DFM (E<sup>d</sup>) monomers in DFM-MeOH complex geometry and Enthalpy of formation ( $\Delta H$ )<sup>f</sup> and Gibbs free energy in kcal/mol**

Conformer	BE <sup>a</sup>	( $\Delta E^{\text{CP}}$ ) <sup>b</sup>	E <sup>c</sup> (MeOH)	E <sup>d</sup> (DFM)	$\Delta G$ <sup>e</sup>	( $\Delta H$ ) <sup>f</sup>
$\sigma$ -type	-3.16	-385273.8280	-72629.4694	-312641.1984	5.63817	-1.97038
$\pi$ -type	-1.89	-385272.6287	-72629.4786	-312641.2611	5.65762	-0.75113

<sup>a</sup>binding energy, <sup>b</sup>counterpoise energy, <sup>c</sup>Energy of Methanol, <sup>d</sup>Energy of DFM, <sup>e</sup>Gibbs free energy and <sup>f</sup>enthalpy of formation

The Figures 3.5 and 3.6 show different hydrogen bonding configurations:  $\sigma$ -type and  $\pi$ -type hydrogen bonding schemes respectively.

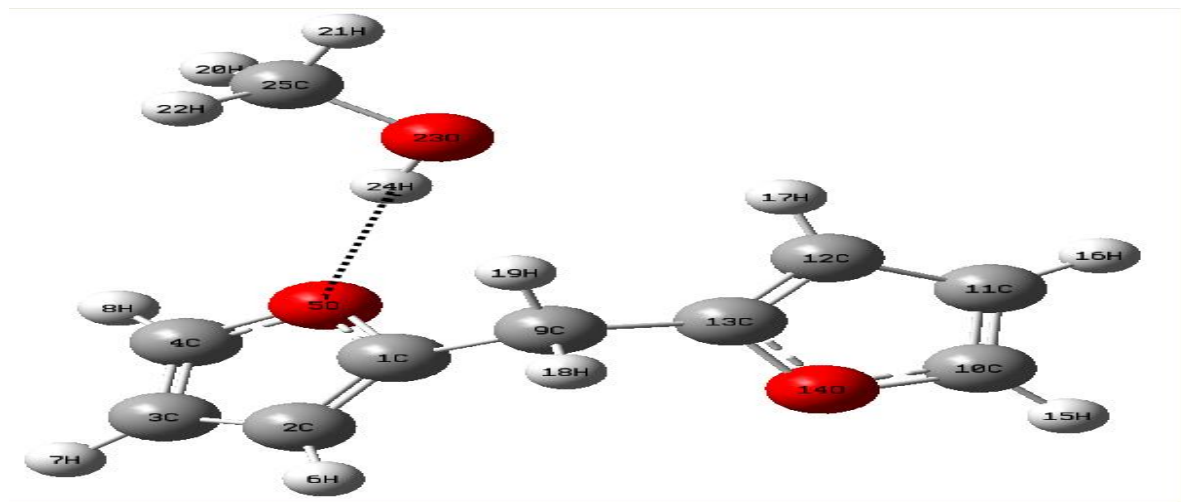


**Figure 3.5:  $\sigma$ -type hydrogen bonding as calculated at B3LYP+G(3d,3p) level of theory**



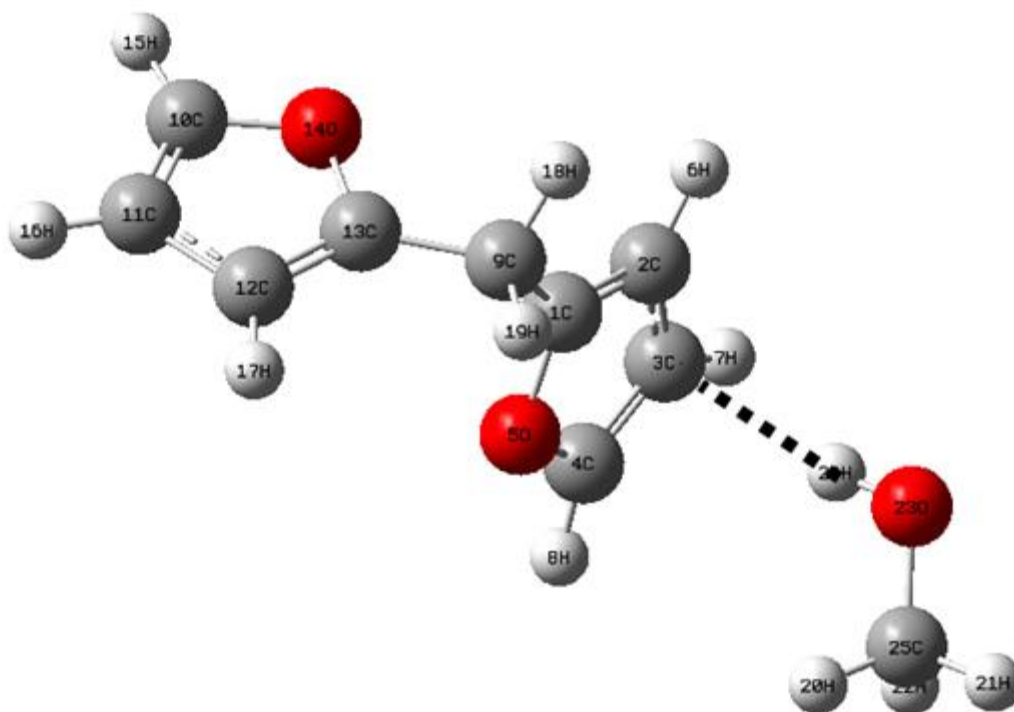
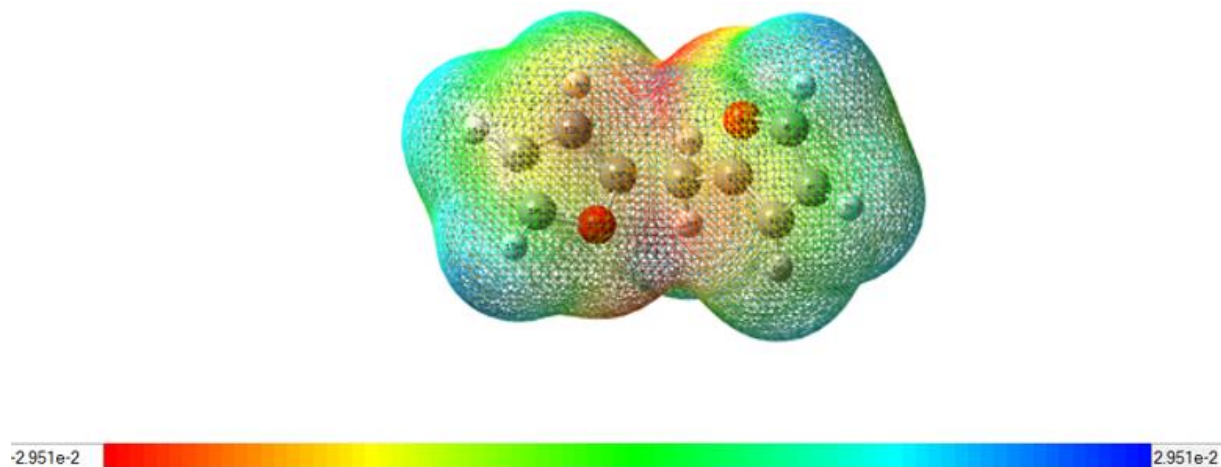


Figure 3.6:  $\pi$ -type hydrogen bonding scheme as calculated at B3LYP+G 6-31(3d, 3p) level of theory

### 3.4.1 Molecular electrostatic potential map

The molecular electrostatic potential (MEP) map in Figure 3.7 is portrayed in a colour coding gradient, whereby the red shade is the most robust electron density region ( $-0.0295$  a.u, more negative zone) and the blue shade is indicative of the less robust charge density ( $+0.0295$  a.u, more positive zone). The MEP map depicted in Figure 3.7 clearly shows that the region above the hetero-atom of DFM is the more electron dense zone, therefore there is higher likelihood for the hydrogen bond to form in these regions than in other regions of the furan moiety. The other site that comprises relatively high density of charge is the region above the furan ring. The nature of charge distribution around the furan moiety can be explained in terms of the presence of lone pair in the hetero-atom and electron resonance in the ring. There is a small delocalization of the lone pair from the hetero-atom to the ring because oxygen is largely electronegative thus it holds more to its electron pair thus making the region around the hetero-atom to have high charge density. Similarly the area around the ring is somehow rich in charge density due to resonance.



**Figure 3.7: Molecular electrostatic potential map (MEP) OF DFM**

### 3.4.2 Potential Energy Surface (PES) Scan

A rigid PES scan was performed which consists of single point energy evaluation over a rectangular grid involving selected internal coordinates on complex A (DFM-MeOH complex) associated with  $\sigma$ -type hydrogen bonding. Only Six (6) possible steps at an incremental angle of  $60^\circ$  were generated. The rigid scan operation (job) was performed by varying the dihedral angle in atoms (25, 23, 24, and 5) within the DFM-MeOH complex. A one dimensional potential energy surface was generated by plotting the values of potential energy and corresponding dihedral angle as depicted in Figure 3.8. It was established that the minimum energy of rigid scan in a plotted potential energy surface (structure  $\sigma$ -type complex) is 0 kcal/mol (before employing thermal energy and Basis set superposition error (BSSE) corrections) and its corresponding dihedral angle of  $-120^\circ$ . The values for potential energy surface are displayed in Table 3.10.

An equilibrium structure or local minimum was obtained following the complexation reaction between DFM and MeOH. It was pre-eminent to probe the potential energy surface of this system for possible global minimum state. This is done by tweaking the dihedral angle  $\Theta$  (25, 23, 24, 5) of the complex with respect to change in single point energy. At first during the preliminary or exploratory phase a relaxed energy scan was performed but the job did not converge and it was aborted. Thereto the rigid scan procedure was adopted.

A relaxed scan was performed upon the  $\pi$ -type complex (The  $\pi$ -type hydrogen bond structure) in order to determine the global minimum within this region of potential energy surface by varying the dihedral angle at 31 steps. The relaxed scan is plotted in Figure 3.9 and the scan coordinates are shown in Table 3.11.

The global minimum (most stable configuration) computed from the PES scan was set to 0.000 kcal/mol. Thus the comparison between  $\sigma$ -type, and  $\pi$ -type complex gives the absolute energy difference ( $\Delta E$ ) of 1.174 kcal/mol. It can be established that  $\sigma$ -type complex is relatively lower in energy, than  $\pi$ -type complex supporting the hypothesis that the  $\sigma$ -type configuration possesses larger binding energy (absolute value) than that founding  $\pi$ -type configuration

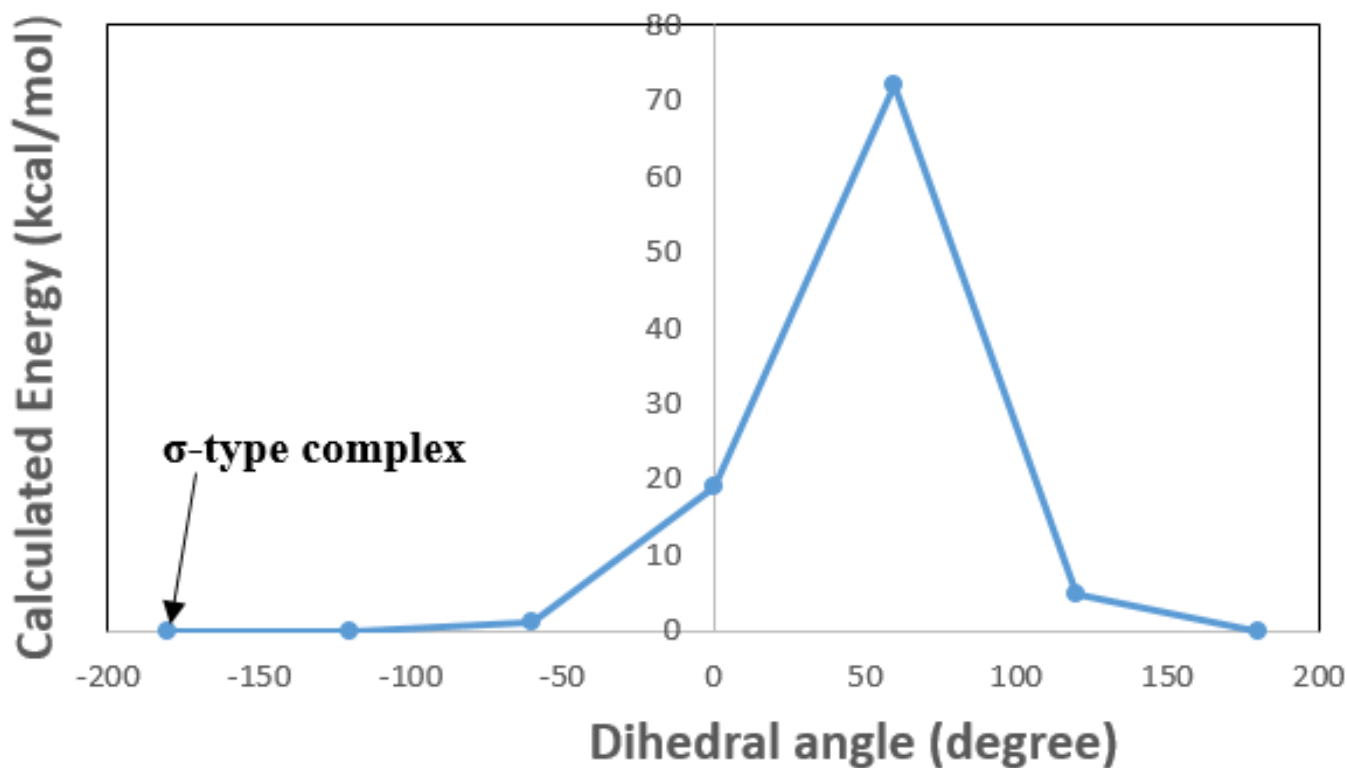


Figure 3.8: Potential energy surface of Complex A

**Table 3.10: Potential energy data points  $\sigma$ -type (structure A) furan-methanol complex obtained by performing rigid (manual) scan**

$\Theta$ (Degrees)	$\Delta E_{\text{total}}$ (kcal/mol)
-180	0.0872
-120	0.000 <sup>a</sup>
-60	1.1729
0	18.9982
60	72.157
120	4.8144
180	0.0872

<sup>a</sup> Global minimum energy of Rigid scan

**Table 3.11: Potential energy data points  $\pi$ -type (structure B) furan-methanol complex obtained by performing redundant scan**

Computational step	$\Delta E_{\text{total}}$ (kcal/mol)
1	0.3332
2	0.0081
3	0.000 <sup>a</sup>
4	0.0012
5	0.0207
6	0.0508
7	0.0922
8	0.1424
9	0.2033
10	0.278
11	0.3602
12	0.4424
13	0.5271
14	0.6187
15	0.2573
16	0.2303
17	0.2108
18	0.1976
19	0.1882
20	0.1851
21	0.1901
22	0.2014
23	0.2196
24	0.2736
25	0.3024
26	0.325
27	0.3313
29	0.3282
30	0.3213
31	0.3182

<sup>a</sup> global minimum energy on the redundant scan

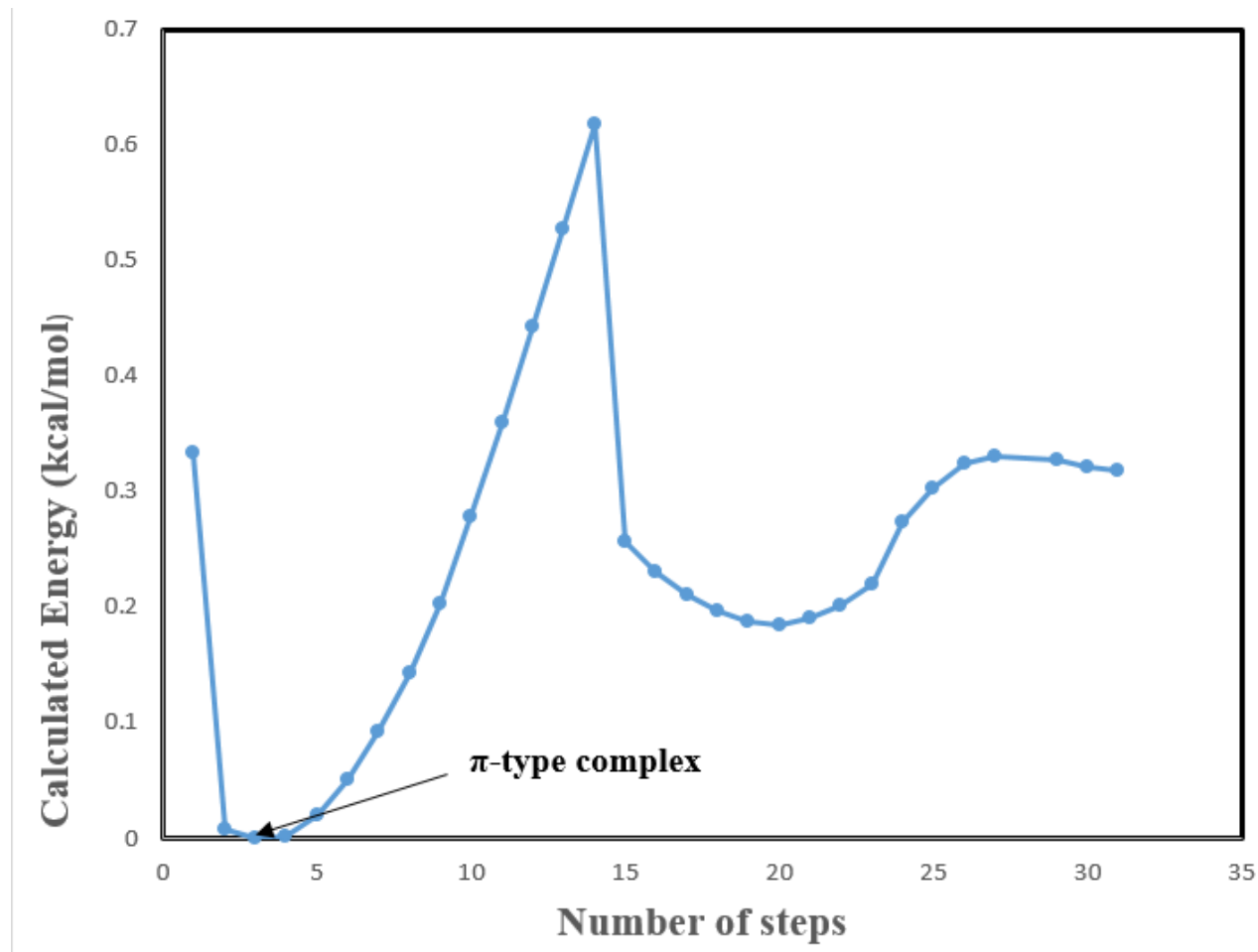


**Figure 3.9: Relaxed energy scan profile**

Rigid and relaxed potential energy scans DFM-MeOH complex are displayed in Figure 3.8 and 3.9 respectively. The relative minimum energy in rigid scan and relaxed energy scan was set to 0.000 kcal/mol and the discrepancy between the two minima is 1.1737 kcal/mol

### 3.4.3 Natural Bond Orbital Analysis

The energy gap between HOMO (DFM) and LUMO (MeOH) determines the overlapping strength between the two frontier orbitals. Thus we can mention two types of hydrogen bonding interactive schemes, namely  $\sigma$ -type and  $\pi$ -type hydrogen bonding. In the first configuration ( $\sigma$ -type) we observe hydrogen bond transfer from donor orbital ( $\sigma^*$  or O-H<sub>methanol</sub>) towards heteroatom (O, lone pair) acceptor orbital. The magnitude of overlap between bonding NBO and antibonding NBO frontier orbitals can be measured using second order perturbation energy  $E_{ij}^2$ .

$$E_{ij}^2 = -2 F_{ij} / \Delta E_{ij} \quad (3.4)$$

Where  $\Delta E_{ij} = E_i - E_j$  is the difference in energy between the interacting molecular orbitals  $i$  and  $j$ ,  $F_{ij}$  is the Fock matrix elements for the interaction between orbitals  $i$  and  $j$  [84]–[88].

We have two types of interactive schemes for hydrogen bonding, but the  $\pi$ -type configuration occurs at C<sub>2</sub> and C<sub>3</sub> on both sides of the furanic ring. Judging from the magnitude of second perturbative energy, the  $\sigma$ -type configuration is the most stable energy structure with second perturbative energy equivalent to 4.55 kcal/mol in contrast to 2.79 kcal/mol as listed in Table 3.11, energy associated with the most stable  $\pi$ -type configuration. Since second order stabilization energy is a measure of electron delocalization or hydrogen bonding, it is quite evident that complex A ( $\sigma$ -type hydrogen bonding configuration) is strongly stabilized by hydrogen bonding than complex B ( $\pi$ -type hydrogen bonding configuration).

The charges on basic oxygen atom of furan around the acidic hydrogen of MeOH within the complex A was calculated as -0.47892 a.u and +0.5127 a.u respectively as depicted in Table 3.12. In complex B the C (2) of furan and acidic proton of Methanol hydroxyl group have atomic charges -0.35129 a.u and 0.50183 a.u respectively. This atomic charge values signify that complex A has more profound electron density transfer than complex B; thus supporting the hypothesis that Complex A is strongly hydrogen bonded.

The redundant energy scan calculations yield two possible equilibrium structures for  $\pi$ -type configuration occurring between acidic proton of methanol and carbon 2 and 3 ( $\beta$ -carbons) of DFM

with relative equilibrium energies of 0.000 kcal/mol for both complexes and their absolute energy differences of 1.1737 kcal/mol. But preferentially the interaction between methanol and carbon 2 of DFM is the global minimum. General inspection of the MEP map of DFM molecule shows that the region around the furanic ring of DFM is clustered with charge density characterized by colour shading gradient ranging from yellow to orange shades and it is apparent that the region associated with carbon 2 of the furanic ring has more charge density when compared to the region above carbon 3. This could be primarily due to the close proximity of this region to the highly electron dense carbon number 1 that receives shuttle of electrons from the adjacent methylene carbon within the structure of DFM, this proximal methylene group determines the direction of flow of electrons. Thus some of the charge density from this region is smeared around the region above carbon 2. Furthermore the  $\beta$ -carbons are preferred binding sites in the furanic ring of DFM in contrast to the centre of the ring because due to resonance structures obtained following electron delocalization, a negative charge is localized in the positions of two  $\beta$ -carbons of the ring. This positioning of negative charge in the  $\beta$ -carbons increases the charge density within these positions thus making them more susceptible to hydrogen bonding. Moreover there is competition happening at this two binding sites of the ring for acid proton of methanol, but carbon-2 is most favoured as there is preferential smearing of charge density around this region arising from proximity to the methylene group directing the flow of electron resonance in a clockwise direction.

**Table 3.12: The stabilization energy, Fock-matrix and energy gap between HOMO and LUMO orbitals**

Configuration type	$E_i - E_j$ (kcal/mol)	$F_{ij}$ (kcal/mol)	$E_{ij}^2$ (kcal/mol)
$\sigma$ -type	1.09	0.063	4.55
$\pi$ -type	0.77	0.043	2.79

**Table 3.13: The atomic charges of DFM-MeOH complex**

Atom	Atomic Charge (a.u)
O(5)	-0.47892
H(24)	+0.5127
C(2)	-0.35129
H(24)	+0.50183



## 4 SUMMARY & CONCLUSIONS

The objectives of this work was to study the structural parameters and properties of DFM and DFM-MeOH complexes. The nature of intermolecular interactions between the two monomers; DFM and MeOH using computational simulations.

In this work the electronic structure properties of DFM and DFM-MeOH Complex was probed using DFT-calculations in order to determine the nature of intermolecular interactions within the DFM-MeOH Complex: two types of hydrogen bond configurations were succinctly obtained. The type-1 configuration depicts hydrogen bonding between acidic proton in MeOH and the hetero atom of furan ring moiety and the type-2 configuration is the interaction between the acidic proton of MeOH and the polarized  $\pi$ -system. This illustration apparently shows that the predominant local minima structure is the type-1 configuration hydrogen bonding. In the previous experimental work in our research laboratory dipole-dipole interaction between the molecular fragments was suggested as the possible intermolecular forces in DFM-MeOH binary solution obtained using excess volumetric properties by density measurements throughout the molar composition.

In our computational calculations we looked at binding energy profile and natural bond orbitals to calculate the stabilization energetics between DFM-MeOH complexes. The later suggested that the nature of intermolecular forces within the dimeric structure of DFM and Methanol is largely hydrogen bonding of classical and non-classical hydrogen bonding type.

## References

- [1] P. J. Atkins, P. De, *Physical chemistry*, 6th editio. Oxford, UK: Oxford University Press, 2006.
- [2] C. Tanford, C. Tanford, J. G. Kirkwood, and J. G. Kirkwood, 'Theory of Protein Titration Curves. I. General Equations for Impenetrable Spheres', *J. Am. Chem. Soc.*, vol. 79, no. 3, pp. 5333–5339, 1957.
- [3] N. Prabhu and K. Sharp, 'Protein-solvent interactions', *Chem. Rev.*, vol. 106, no. 5, pp. 1616–1623, 2006.
- [4] M. Krishnan, 'A simple model for electrical charge in globular macromolecules and linear polyelectrolytes in solution', *J. Chem. Phys.*, vol. 146, no. 20, 2017.
- [5] O. Mokate and W. A. A. Ddamba, 'Volumetric Properties of Difurylmethane in Methanol from 288 . 15 to 308 . 15 K', *J. Solution Chem.*, vol. 34, no. 11, pp. 1327–1339, 2005.
- [6] O. Mokate and W. A. A. Ddamba, 'Effect of Temperature on the Volumetric Properties of [ Difurylmethane + ( C 2 – C 6 ) Alkan-1-ol ] Binary Systems : Analyses of New and Literature Density Data in the Temperature Range 288 . 15 – 308 . 15 K', *J. Solution Chem.*, pp. 331–350, 2008.
- [7] B. T. Mmereki, I. Oathotse, and W. A. A. Ddamba, 'Ultrasonic speeds and isentropic compressibilities of {difurylmethane + (C1-C6) n-alkanol} binary mixtures at T = 298.15 K', *J. Chem. Thermodyn.*, vol. 42, no. 11, pp. 1346–1351, 2010.
- [8] G. C. Benson and O. Kiyohara, 'Thermodynamics of aqueous mixtures of nonelectrolytes. I. Excess volumes of water-n-alcohol mixtures at several temperatures', *J. Solution Chem.*, vol. 9, no. 10, pp. 791–804, 1980.
- [9] G. Douheret and M. I. Davis, 'Measurement, Analysis, and Utility of Excess Molar -', *Chem. Soc. Rev.*, vol. 22, no. 434, pp. 43–50, 1971.
- [10] M. I. Davis, 'Partial Excess Molar Properties of Water in Amphiphile Plus Water-Systems', *Thermochim. Acta*, vol. 200, pp. 15–31, 1992.
- [11] T. C. Bai, J. Yao, and S. J. Han, 'Excess molar volumes for the ternary mixture N,N-dimethylformamide + methanol + water at the temperature 298.15 K', *J. Chem. Eng. Data*, vol. 44, no. 3, pp. 491–496, 1999.
- [12] F. N. Dunlop, A.P., Peters, *The Furans*. New York, USA: Reinhold Publishing Co, 1953.
- [13] T. A. Nevolina, T. A. Stroganova, M. V Shevlyakov, and A. V Butin, 'Synthesis of amines

- of the di- and trifurylmethane series', *Chem. Heterocycl. Compd.*, vol. 43, no. 4, pp. 505–512, 2007.
- [14] K. Ji, Y. Shen, X. Shu, and H. Xiao, 'Synthesis of Difurylmethane Derivatives via the Gold-Catalyzed', *Adv.Synth. Catal.*, pp. 1275–1280, 2008.
- [15] B. T. O. M. Sidney and F. Winmill, 'q = Sl c =', *J. Chem. Soc. Trans*, vol. 101, pp. 1635–1676, 1912.
- [16] T. H. E. Standpoint, 'most of the fixed oxygen was removed while the hydrocarbon content was not much altered, the differences observed are more likely due to this latter cause. Conclusions.', vol. 453, no. 1899, pp. 1419–1433, 1920.
- [17] E. Arunan, G. R. Desiraju, R. A. Klein, J. Sadlej, S. Scheiner, I. Alkorta, D. C. Clary, R. H. Crabtree, J. J. Dannenberg, P. Hobza, H. G. Kjaergaard, A. C. Legon, B. Mennucci, and D. J. Nesbitt, 'Definition of the hydrogen bond ( IUPAC Recommendations 2011 )\*', vol. 83, no. 8, pp. 1637–1641, 2011.
- [18] J. Phillips, B. Xia, and J. A. Menéndez, 'Calorimetric study of oxygen adsorption on activated carbon', *Thermochim. Acta*, vol. 312, no. 1–2, pp. 87–93, 1998.
- [19] Louis J Farrugia, 'No Title' . .
- [20] M. Prakash, K. G. Samy, and V. Subramanian, 'Benzene–Water (BZW<sub>n</sub> ( n = 1 – 10)) Clusters', *J. Phys. Chem. A*, vol. 113, no. 50, pp. 13845–13852, Dec. 2009.
- [21] S. V. Prakash.M, Gopal Samy.K, 'Benzene-Water ( BZW<sub>n</sub> ( n = 1-10 )) Clusters', *J. Phys. Chem. A*, vol. 113, no. 50, pp. 13845–13852, 2009.
- [22] T. Emilsson, H. S. Gutowsky, G. De Oliveira, and C. E. Dykstra, 'Rotational patches : Stark effect , dipole moment , and dynamics of water loosely bound to benzene Rotational patches : Stark effect , dipole moment , and dynamics of water loosely bound to benzene', *J. Chem. Phys.*, vol. 1287, no. 2000, 2014.
- [23] T. Desiraju, G. R.; Steiner, 'The Weak Hydrogen Bond in Structural Chemistry and Biology', Oxford,NY: Oxford University Press Inc, 1999.
- [24] G. A. Jeffrey, *An Introduction to Hydrogen Bonding*. Oxford, NY: Oxford University Press, 1997.
- [25] T. Steiner and G. R. Desiraju, 'Distinction between the weak hydrogen bond and the van der Waals interaction', *Chem. Commun.*, no. 8, pp. 891–892, 1998.
- [26] J. K. Gregory, 'The dipole moment of the water dimer', *Chem. Phys. Lett.*, vol. 282, no. 2,

- pp. 147–151, 1998.
- [27] J. K. Gregory, D. C. Clary, K. Liu, M. G. Brown, and R. J. Saykally, ‘The water dipole moment in water clusters’, *Science* (80-. ), vol. 275, no. 5301, pp. 814–817, 1997.
- [28] A. A. Vostrikov, D. Y. Dubov, and S. V. Drozdov, ‘Dipole moment of water clusters and the greenhouse effect’, *Tech. Phys. Lett.*, vol. 34, no. 3, pp. 221–224, 2008.
- [29] D. Kaur and S. Khanna, ‘Intermolecular hydrogen bonding interactions of furan , isoxazole and oxazole with water’, *Comput. Theor. Chem.*, vol. 963, no. 1, pp. 71–75, 2011.
- [30] J. Wu, H. Yan, H. Chen, A. Zhong, and W. Cao, ‘Insight into the nature of the interactions of pyridine , funan and thiophene with LiNH<sub>2</sub>’, *Comput. Theor. Chem.*, vol. 1000, pp. 52–59, 2012.
- [31] D. Xie and J. Li, ‘Molecular Design’, *Internet Electron. J. Mol. Des.*, pp. 306–314, 2003.
- [32] J. A. Sordo, ‘On the use of the Boys ± Bernardi function counterpoise procedure to correct barrier heights for basis set superposition error q’, vol. 537, pp. 245–251, 2001.
- [33] O. H. Cl, H. Zhao, S. Tang, Q. Zhang, and L. Du, ‘RSC Advances Weak hydrogen bonding competition between O –’, *RSC Adv.*, vol. 7, pp. 22485–22491, 2017.
- [34] D. L. Howard and H. G. Kjaergaard, ‘Vapor Phase near Infrared Spectroscopy of the Hydrogen Bonded Methanol - Trimethylamine Complex’, *J Phys Chem*, pp. 9597–9601, 2006.
- [35] M. Heger, R. A. Mata, and M. A. Suhm, ‘Chemical Science ethene prototype under experimental and theoretical scrutiny’, *Chem. Sci.*, vol. 6, pp. 3738–3745, 2015.
- [36] E. E. Fileti and S. Canuto, ‘Calculated infrared spectra of hydrogen-bonded methanol-water, water-methanol, and methanol-methanol complexes’, *Int. J. Quantum Chem.*, vol. 104, no. 5, pp. 808–815, 2005.
- [37] M. Hippler, ‘Quantum chemical study and infrared spectroscopy of hydrogen-bonded CHCl<sub>3</sub>-NH<sub>3</sub> in the gas phase.’, *J. Chem. Phys.*, vol. 127, no. 8, p. 084306, 2007.
- [38] S. L. Buchwalter, ‘The Polymerization of Furfuryl Acetate in Acetonitrile’, *J. Polym. Sci.*, vol. 23, pp. 2897–2911, 1985.
- [39] J. P. Desclaux, ‘Hartree Fock Slater Self Consistent Field Calculations’, *Comput. Phys. Commun.*, vol. 1, pp. 216–222, 1969.
- [40] H. Fock, S. Self, C. Field, C. J. P. Desclaux, P. C. Deshmukh, A. Banik, and D. Angom, ‘Hartree-Fock Self-Consistent Field Method for Many-Electron Systems’, vol. 1, no.

- November, pp. 216–222, 1969.
- [41] R. Van Leeuwen, J. Neugebauer, L. Visscher, and F. M. Bickelhaupt, ‘Editorial for PCCP themed issue “developments in Density Functional Theory”’, *Phys. Chem. Chem. Phys.*, vol. 18, no. 31, pp. 20864–20867, 2016.
- [42] H. Soscún, J. Hernández, R. Escobar, C. Toro-Mendoza, Y. Alvarado, and A. Hinchliffe, ‘Ab initio and density functional theory calculations of the dipole polarizability and the second dipole hyperpolarizability of benzene’, *Int. J. Quantum Chem.*, vol. 90, no. 2, pp. 497–506, 2002.
- [43] H. O. Di Rocco, F. Lanzini, and J. C. Aguiar, ‘Thomas–Fermi approach to density functional theory: binding energy for atomic systems’, *Eur. J. Phys.*, vol. 37, no. 6, p. 065402, 2016.
- [44] B. G. Johnson, P. M. W. Gill, and J. A. Pople, ‘The performance of a family of density functional methods’, *J. Chem. Phys.*, vol. 98, pp. 5612–5626, 1993.
- [45] P. N. Ma, S. Pilati, M. Troyer, and X. Dai, ‘Density functional theory for atomic Fermi gases’, *Nat. Phys.*, vol. 8, no. 8, 2012.
- [46] R. G. Parr and S. K. Ghosh, ‘Thomas-Fermi theory for atomic systems’, *Proc. Natl. Acad. Sci.*, vol. 83, no. 11, pp. 3577–3579, 1986.
- [47] L. C. Cune and M. Apostol, ‘On the atomic binding energy in the Thomas-Fermi model’, *Rom. Reports Phys.*, vol. 55, no. 9–10, pp. 913–919, 2010.
- [48] K. K. Baldridge and M. S. Gordon, ‘Potentially Aromatic Metallocycles’, *J. Am. Chem. Soc.*, vol. 110, no. 34, pp. 4204–4208, 1988.
- [49] Y. G. Byun, S. Saebo, and C. U. Pittman, ‘An Ab Initio Study of Potentially Aromatic and Antiaromatic Three-Membered Rings’, *J. Am. Chem. Soc.*, vol. 113, no. 10, pp. 3689–3696, 1991.
- [50] L. H.-N. B. Bak, D. Christensen, W B. Dixon and M. S. J. R Andersen, ‘The Complete Structure of Furan’, *J. Mol. Spectrosc.*, vol. 129, pp. 124–129, 1962.
- [51] G. Maroulis, ‘Applying conventional Ab initio and density functional theory approaches to electric property calculations. Quantitative aspects and perspectives’, *Struct. Bond.*, vol. 149, pp. 95–130, 2012.
- [52] S. Millefiori and A. Alparone, ‘(Hyper)polarizability of chalcogenophenes C<sub>4</sub>H<sub>4</sub>X (X = O, S, Se, Te) Conventional ab initio and density functional theory study’, *J. Mol. Struct.*, vol.

- 1280, pp. 59–78, 1998.
- [53] J. Lii and N. L. Allinger, ‘Systematic Comparison of Experimental, Quantum Mechanical, and Molecular Mechanical Bond Lengths for Organic Molecules’, *J. Chem. Phys.*, vol. 3654, no. 95, pp. 8763–8769, 1996.
- [54] H. U. Suter, ‘Comparison between Optimized Geometries and Vibrational Frequencies Calculated by the DFT Methods’, *J. Chem. Phys.*, vol. 3654, no. 96, pp. 15056–15063, 1996.
- [55] A. H. Ta and J. M. Sosctin, ‘Ab initio studies of the dipole polarizabilities of conjugated molecules. Part 5. The five-membered heterocyclics C<sub>4</sub>H<sub>4</sub>E (E = BH, AlH, CH<sub>2</sub>, SiH<sub>2</sub>, NH, PH, O and S)’, *J. Mol. Struct.*, vol. 1, pp. 109–125, 1995.
- [56] F. H. Allen, O. Kennard, D. G. Watson, L. Brammer, A. G. Orpen, and R. Taylor, ‘Bond Lengths in Organic Compounds’, *J. Chem. Soc., Perkin Trans. 2*, pp. S1–S19, 1987.
- [57] B. Ma, J.-H. Lii, H. F. Schaefer III, and N. L. Allinger, ‘Systematic comparison of experimental, quantum mechanical, and molecular mechanical bond lengths for organic molecules’, *J. Phys. Chem.*, vol. 100, no. 21, pp. 8763–8769, 1996.
- [58] J. L. Toto, T. T. Toto, and C. P. De Melo, ‘A comparative study of the effect of electron correlation in the hyperpolarizability of polyyne, polyacetylene and polypyrrole oligomers’, *Chem. Phys. Lett.*, vol. 4, no. November, pp. 2–6, 1995.
- [59] P. A. Limacher, Q. Li, and H. P. Lüthi, ‘On the effect of electron correlation on the static second hyperpolarizability of conjugated oligomer chains’, *J. Chem. Phys.*, vol. 135, no. 1, 2011.
- [60] D. R. Beck and C. A. Nicolaides, ‘The effect of electron correlation on atomic properties’, *Int. J. Quantum Chem.*, vol. 8, no. 8 S, pp. 17–28, 1974.
- [61] G. Maroulis and A. J. Thakkar, ‘How important is electron correlation for the hyperpolarizability of ethyne?’, *J. Chem. Phys.*, vol. 93, no. 1, pp. 652–656, 1990.
- [62] M. H. Sirvetz, ‘The Microwave Spectrum of Furan’, *J. Chem. Phys.*, vol. 19, no. 12, pp. 1609–1610, 1951.
- [63] N. E. Kassimi, R. J. Doerksen, and A. J. Thakkar, ‘Polarizabilities of oxazoles: ab initio calculations and simple models’, *J Phys Chem*, vol. 100, no. 95, pp. 8752–8757, 1996.
- [64] Z. G. Keolopile, M. Gutowski, and M. Haranczyk, ‘Discovery of Most Stable Structures of Neutral and Anionic Phenylalanine through Automated Scanning of Tautomeric and

- Conformational Spaces', *J. Chem. Theory Comput.*, 2013.
- [65] E. D. Simandiras, N. C. Handy, and R. D. Amos, 'Correlated ab Initio Harmonic Frequencies and Infrared Intensities for Furan, Pyrrole, and Thiophene', *J Phys Chem*, no. 17, pp. 1739–1742, 1988.
- [66] V. Barone, 'Vibrational spectra of large molecules by density functional computations beyond the harmonic approximation : the case of pyrrole and furan', *Chem. Phys. Lett.*, vol. 383, pp. 528–532, 2004.
- [67] C. Cappelli, S. Monti, G. Scalmani, and V. Barone, 'On the calculation of vibrational frequencies for molecules in solution beyond the harmonic approximation', *J. Chem. Theory Comput.*, vol. 6, no. 5, pp. 1660–1669, 2010.
- [68] D. Oschetzki, M. Neff, P. Meier, F. Pfeiffer, and G. Rauhut, 'Selected Aspects Concerning the Efficient Calculation of Vibrational Spectra beyond the Harmonic Approximation', *Croat. Chem. Acta*, vol. 85, no. 4, pp. 379–390, 2012.
- [69] p.s. Kalsi, *Spectroscopy of Organic Compounds*, 6th ed. New Delhi: springfield, VA, U.S.A, 1993.
- [70] J. D. Magdaline and T. Chithambarathanu, 'Natural bond orbital analysis and vibrational spectroscopic studies of 2-furoic acid using density functional theory', *Indian J. Pure Appl. Phys.*, vol. 50, no. January, pp. 7–13, 2012.
- [71] M. Ackermann, M. Kudra, F. Billes, and H. Bo, 'A vibrational spectroscopic study on furan and its hydrated derivatives', *J. Mol. Struct.*, vol. 672, pp. 1–16, 2004.
- [72] A. H. Cowley, J. E. Kilduff, N. C. Norman, M. Pakulski, J. L. Atwood, and W. E. Hunter, 'Electrophilic Additions to Diphosphenes (RP=PR)', *J. Am. Chem. Soc.*, vol. 105, no. 14, pp. 4845–4846, 1983.
- [73] E. J. Borkowski, F. D. Suvire, and R. D. Enriz, 'Journal of Molecular Structure : THEOCHEM Advances in correlation between experimental and DFT / GIAO computed C NMR chemical shifts : A theoretical study on pentacyclic terpenoids ( fernenenes )', *J. Mol. Struct. THEOCHEM*, vol. 953, no. 1–3, pp. 83–90, 2010.
- [74] D. A. Forsyth and A. B. Sebag, 'Computed 13 C NMR Chemical Shifts via Empirically Scaled GIAO Shieldings and Molecular Mechanics Geometries . Conformation and Configuration from 13 C Shifts', *J. Am. Chem. Soc.*, vol. 7863, no. c, pp. 9483–9494, 1997.
- [75] G. M. Sheldrick, 'Crystal structure refinement with SHELXL', *Acta Crystallogr. Sect. C*

- Struct. Chem.*, vol. 71, no. Md, pp. 3–8, 2015.
- [76] A. D. Becke, ‘Density-functional thermochemistry. III. The role of exact exchange’, *J. Chem. Phys.*, vol. 98, no. 7, pp. 5648–5652, 1993.
- [77] W. Koch and M. C. Holthausen, *A Chemist’s Guide to Density Functional Theory*, vol. 3. 2001.
- [78] L. Du, ‘Matrix isolation FTIR study of hydrogen-bonded complexes of methanol with heterocyclic organic compounds complexes of methanol with heterocyclic organic’, *RSC Adv.*, vol. 7, no. January 2017, pp. 2503–2512, 2016.
- [79] O. W. Kgagodi and F. Mbaiwa, ‘Molecular dynamics study of 2,2’-difurylmethane and n-propanol binary mixture’, *J. Mol. Liq.*, vol. 17, pp. 30481–30491, 2016.
- [80] B. G. Oliveira, E. M. Duarte, R. C. M. U. Araújo, M. N. Ramos, and A. B. Carvalho, ‘A theoretical study of nonlinearity in heterocyclic hydrogen-bonded complexes’, *Spectrochim. Acta - Part A Mol. Biomol. Spectrosc.*, vol. 61, no. 3, pp. 491–494, 2005.
- [81] A. M. Priya, L. Senthilkumar, and P. Kolandaivel, ‘Hydrogen-bonded complexes of serotonin with methanol and ethanol: A DFT study’, *Struct. Chem.*, vol. 25, no. 1, pp. 139–157, 2014.
- [82] M. K. Van Bael, J. Smets, K. Schoone, L. Houben, W. McCarthy, L. Adamowicz, M. J. Nowak, and G. Maes, ‘Matrix-isolation FTIR studies and theoretical calculations of hydrogen-bonded complexes of imidazole. A comparison between experimental results and different calculation methods’, *Journal of Physical Chemistry A*, vol. 101, no. 13. pp. 2397–2413, 1997.
- [83] S. B. H. Bach and B. S. Ault, ‘Infrared matrix isolation study of the hydrogen-bonded complexes between formaldehyde and the hydrogen halides and cyanide’, *J. Phys. Chem.*, vol. 88, no. 16, pp. 3600–3604, 1984.
- [84] G. P. Bean, ‘Application of Natural Bond Orbital Analysis and Natural Resonance Theory to Delocalization and Aromaticity in Five-Membered Heteroaromatic Compounds’, *J. Org. Chem.*, vol. 3263, no. 97, pp. 2497–2506, 1998.
- [85] J. P. Foster and F. Weinhold, ‘Natural Hybrid Orbitals’, *J. Am. Chem. Soc.*, vol. 4, no. 22, pp. 7211–7218, 1980.
- [86] A. E. Reed, L. A. Curtiss, and F. Weinhold, ‘Intermolecular Interactions from a Natural Bond Orbital, Donor-Acceptor Viewpoint’, *Chem. Rev.*, no. 88, pp. 899–926, 1988.



- [87] L. Goodman and R. R. Sauer, 'Diffuse functions in natural bond orbital analysis', *J. Comput. Chem.*, vol. 28, no. 1, pp. 269–275, 2007.
- [88] A. J. Pounds, 'Valency and Bonding: A Natural Bond Orbital Donor–Acceptor Perspective (Frank Weinhold and Clark Landis)', *J. Chem. Educ.*, vol. 84, no. 1, p. 43, 2007.

## Appendices:

### Appendix A. Conformers of DFM

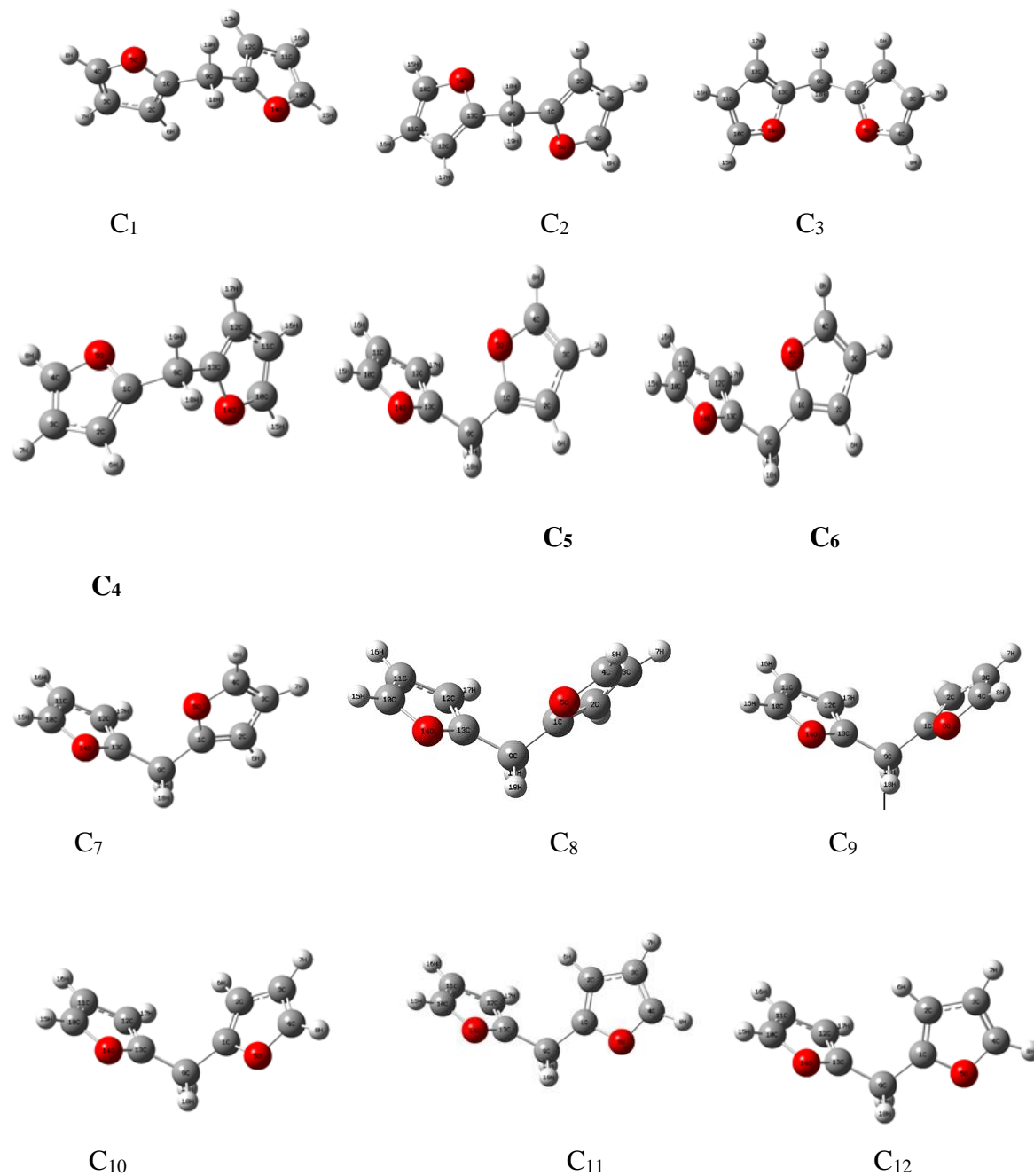
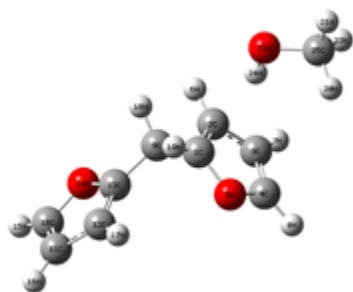
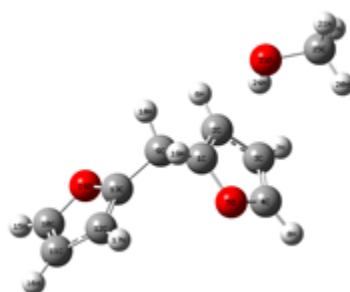


Figure A 1: Conformational structures of DFM

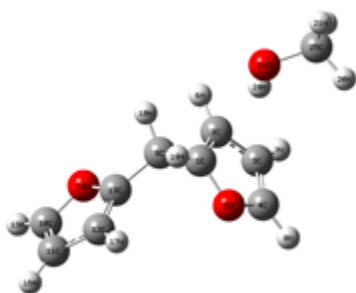
**Appendix B. Conformers of DFM-Methanol obtained from relaxed potential energy scan**



**C<sub>1B</sub>**



**C<sub>2B</sub>**



**C<sub>3B</sub>**

**Figure B 1: Conformers of DFM-MeOH Complex 1**